

Conformal Dimensions On Causal Random Geometry

Ryan Barouki, Henry Stubbs, John Wheeler

*Rudolf Peierls Centre for Theoretical Physics, Department of Physics,
Parks Road, Oxford, OX1 3PU*

E-mail: ryan.barouki@physics.ox.ac.uk

ABSTRACT: We investigate the interaction between matter and causal dynamical triangulations (CDT) in the context of two-dimensional quantum gravity. We focus on the Ising model coupled to CDT, contrasting this with Liouville gravity and the relation to the Knizhnik-Polyakov-Zamolodchikov (KPZ) formula. We demonstrate analytically for the quenched model that the conformal dimensions of fields on CDT align with those on a fixed lattice. We do this using a combination of lattice methods and adapting the Duplantier-Sheffield framework to CDT, emphasizing the one-dimensional nature of CDT and its description via a stochastic differential equation.

Contents

1	Introduction	1
2	2D quantum gravity	3
2.1	Graphs	4
2.2	Euclidean triangulations	5
2.3	Causal triangulations	6
2.4	Coupling matter	9
2.5	Liouville gravity à la Duplantier-Sheffield	10
3	The Ising model and topological defects	13
3.1	The Ising model in the plaquette formalism	13
3.2	The spin-flip defect	15
3.3	The duality defect	15
3.4	The Ising fusion category	16
3.5	Dehn twist operators on the lattice	17
4	Stochastic formulation of CDT	22
4.1	The Lamperti-Ney Process	22
4.2	Scaling dimensions of Ising CFT fields	24
4.3	Properties of the Lamperti-Ney process	25
4.4	Classical and quantum scaling exponents in CDT	26
5	Connection to Hořava-Lifshitz gravity	29
6	Outlook and extension to the annealed case	30
A	Defects at the boundary	32
B	The domain wall	33

1 Introduction

Random surfaces have been studied thoroughly in the physics literature due to their connection to string theory (the string world-sheet) and conformal field theory. These models are also of interest from a statistical physics point of view. For example, results of various scaling exponents of random walks on a regular \mathbb{Z}^2 lattice were first calculated exactly on a random surface and then mapped to the fixed lattice [1]. In

this paper we think of the random surface as defining “two dimensional quantum gravity”.

When defining quantum gravity, one is free to choose the class of random surfaces over which we sum in a path integral. As we will explain in detail in section 2, one natural choice comes from discretising the Einstein-Hilbert action and “Wick rotating” to Euclidean signature. The path integral then becomes a sum over planar maps which approximate a random surface. We call this class *Liouville random surfaces* for its connection to Liouville gravity which will be explained in the following sections. Matter coupled to Liouville random surfaces has been studied thoroughly in the context of Liouville gravity. One important result is the *Knizhnik-Polyakov-Zamolodchikov* (KPZ) formula [2–4] which relates the scaling dimension x of a conformal field on a flat background to the value Δ on a Liouville random surface. The intuition for why scaling dimensions of fields get shifted is that the highly fractal and singular nature of the underlying geometry (as depicted in figure 1) “dresses” the matter degrees of freedom. For example, the Ising model coupled to Liouville random surfaces has been calculated exactly with matrix model techniques [5, 6] and the scaling dimensions agree with those found with the KPZ formula.

Liouville random surfaces bear many interesting results. One such result is the Hausdorff dimension $d_H = 4$, a dimension that probes the large-scale structure of the space. Many consider this pathological since the aim is to define two-dimensional quantum gravity, where two large dimensions are desirable. These issues first motivated Ambjørn and Loll [7] to consider another class of random surfaces – those which are globally hyperbolic i.e. contain a time slicing. Time slicing is equivalent to including the causal structure in the set of allowed surfaces. This program is thus called *causal dynamical triangulations* (CDT) since it is often implemented as a sum over discrete triangulations.

In this paper, we are interested in how matter couples to CDT – we use the Ising model as an example but the main results can be extended to so-called RSOS, or height models. Not much is known analytically, but numerical studies suggest that the scaling dimensions of the Ising fields are not shifted from their classical values. It was shown using Monte Carlo methods and a high-temperature expansion that the critical exponents of a single Ising model ($c = 1/2$) coupled to CDT appear to retain their classical values [8]. Furthermore, a numerical study of the three-state Potts model ($c = 4/5$) found the same behaviour [9]. Perhaps more surprisingly, in a numerical study of 8 Ising models ($c = 4$) coupled to CDT, the scaling dimensions of the matter fields still remained unchanged despite a change in the gravity sector [10]. It appears that CDT coupled to unitary matter has the universal property that the critical exponents take their classical values and that this result is robust even beyond $c = 1$. Interestingly, it has been found that there are changes to the scaling exponents when coupling hard dimers to CDT in a certain phase of the model [11]. However, the hard dimer model has a central charge $c = -22/5$ and so is non-unitary.

A non-unitary model will contain complex phases and so cannot be described in terms of a positive definite stochastic process. The results of this paper do not apply to such models.

We provide a series of analytical arguments for why the scaling dimensions of fields on CDT are no different to those on a fixed lattice for the quenched model. Crucial to our arguments are the topological defect formulation of the Ising model [12] and evasion of the KPZ relation. The most useful formulation of the latter for our purposes is that of Duplantier-Sheffield (DS) [13] whose framework we adapt to CDT to show that no analogue of KPZ applies. This follows from the fact that CDT is essentially one-dimensional and can be described in terms of a stochastic differential equation (SDE) which has continuous sample paths *almost surely*. As a consequence, KPZ is evaded.

This paper is structured as follows. In section 2 we outline the essential theoretical background for models of 2D quantum gravity, including CDT and the DS approach to Liouville gravity. In section 3 we explain the plaquette formalism of the Ising model as described in [12] and use the algebra of topological defects to find algebraic relations for operators that will be crucial for finding the conformal dimensions: the Dehn twist operators. In section 4 we show that one can indeed construct a Dehn twist in the continuum, from which we calculate the conformal dimensions of the Ising fields. Furthermore, we provide an alternative proof that there will be no KPZ-like relation in continuum CDT by constructing a random measure and following the arguments of DS in [13]. In section 5 we extend the existing connection to Hořava–Lifshitz gravity originally found in [14]. Finally, in section 6 we provide an argument for why our results may apply more generally to the model where the geometry and matter are sampled according to a joint measure (*annealed model*), which relies solely on the continuity of the process describing the evolution of CDT.

2 2D quantum gravity

In Lorentzian space-time, quantum gravity on the two dimensional manifold M is defined by the path integral

$$Z(\Lambda) = \int \mathcal{D}[g] \mathcal{D}[\Phi] e^{iS_{EH}(g) + iS_m(\Phi, g)}. \quad (2.1)$$

Here $[g]$ denotes the equivalence class of Lorentzian metrics g on M up to diffeomorphisms, and $[\Phi]$ the configuration of, for the moment unspecified, matter degrees of freedom living on M . $S_{EH}(g)$ is the Einstein-Hilbert action

$$S_{EH}(g) = \frac{1}{16\pi G_N} \int_M d^2x \sqrt{g} (2\Lambda - R), \quad (2.2)$$

where G_N is Newton's constant, Λ is the cosmological constant, and R is the Ricci scalar curvature. $S_m(\Phi, g)$ is the diffeomorphism invariant action for the matter

degrees of freedom. For simplicity we have omitted the Gibbons-Hawking-York term for manifolds with boundary. We will work with the Euclidean gravity model which is similarly defined by

$$Z(\Lambda) = \int \mathcal{D}[g] \mathcal{D}[\Phi] e^{-S_{EH}(g) - S_m(\Phi, g)}, \quad (2.3)$$

where now the functional integration is over Euclidean, rather than Lorentzian, metrics. Note, however, that the relationship between Lorentzian and Euclidean models cannot be seen as simply making the substitution $t \rightarrow -it$ as in the usual Wick rotation because this transformation does not commute with diffeomorphisms.

In two dimensions, Euclidean manifolds are completely characterised by their genus g and the number of boundaries b . Moreover, the curvature part of the Einstein-Hilbert action is a topological invariant due to the Gauss-Bonnet theorem

$$\int_M d^2x \sqrt{g} R = 4\pi\chi(M), \quad (2.4)$$

where $\chi(M) = 2 - 2g - b$ is the Euler characteristic of the manifold. Hence for a fixed topology, every geometry receives the same factor (2.4) in the path integral and can be factored out leaving only the cosmological constant term, so we henceforth set $8\pi G_N = 1$. The physics of the model then lies largely in the proper definition of the functional integral over the metric. We will be concerned with two (apparently) different methods for doing this: the first is by the explicit discretization of spacetime; and the second by representation in terms of stochastic processes.

2.1 Graphs

Much of this paper is most conveniently expressed in the language of graphs so for convenience we gather our definitions here.

Definition 2.1.

- (i) A simple planar graph $G = (V, E)$ consists of a set of vertices V and a set of edges E that are unordered pairs of distinct vertices $\langle u, v \rangle$, such that no two vertices share more than one edge, and such that G can be embedded in the plane with no two edges intersecting. We denote by $d(u, v)$ the graph distance between vertices u and v .
- (ii) A rooted graph G is a graph with one marked vertex called the root v_0 .
- (iii) The dual graph G^* is constructed from G by placing a vertex in every face, and joining the new vertices with edges such that each new edge intersects only one edge of G . Essentially, vertices are mapped to faces, edges to edges and faces to vertices.
- (iv) A triangulation T is a rooted planar graph where every face is a triangle.
- (v) A tree is planar graph with no cycles.

2.2 Euclidean triangulations

One way to implement the gravitational path integral (2.3) is to discretise space-time and replace the functional integral by a sum over discrete geometries. This approach provides a UV cut-off in the form of the lattice spacing and is naturally non-perturbative. Indeed, the use of generalized triangulations to approximate the geometry of manifolds in general relativity goes back to the work of Regge [15] on coordinate-independent computational methods. Here we focus on the approximation of a two-dimensional manifold M and its geometry g by triangulations composed of piece-wise flat equilateral triangles each of the same area α . Heuristically a given continuum configuration of fixed area A can be approximated progressively more accurately by increasing the number of triangles, N_α , used and decreasing α such that $N_\alpha\alpha = A$ is held fixed. Additionally, for fixed N_α , a given triangulation defines a set of graph distances $\{d(v_i, v_j)\}$ between vertices pairwise that approximates the set of geodesic distances on M ; hence each distinct triangulation approximates a distinct metric g .

We first consider the pure gravitational system with no matter degrees of freedom on a disk M . Then let $\mathcal{E}(M)$ be the set of inequivalent, unrestricted triangulations of M and define the partition function

$$W[\tilde{g}, z] = \sum_{T \in \mathcal{E}(M)} \tilde{g}^{\Delta(T)} z^{|\partial T|}. \quad (2.5)$$

Here we denote by $\Delta(T)$ the number of triangles in T , and by $|\partial T|$ the number of edges in the boundary of T . The combinatorics of $\mathcal{E}(M)$ was first elucidated by Tutte in [16–19]. Crucially the number of triangulations $T \in \mathcal{E}(M)$ such that $\Delta(T) = n$ grows more slowly than \tilde{g}_c^{-n} with $0 < \tilde{g}_c < 1$. It follows that the sum in (2.5) converges and W exists for $\tilde{g} < \tilde{g}_c$.

It was proposed in [20, 21] that the sum over triangulations in (2.5), taken in the limit $\tilde{g} \uparrow \tilde{g}_c$ where arbitrarily large triangulations dominate, can be identified with the Euclidean functional integral over the metric. Setting $\tilde{g} \rightarrow \tilde{g}_c e^{-\Lambda\alpha}$, identifying the area

$$\alpha\Delta(T) \rightarrow \int_{\mathcal{M}} d^2x \sqrt{g}, \quad (2.6)$$

and the triangulation sum

$$\sum_{T \in \mathcal{E}(M)} \frac{1}{C(T)} \tilde{g}_c^{\Delta(T)}(\cdot) \rightarrow \int \mathcal{D}[g](\cdot), \quad (2.7)$$

we see that $W[\tilde{g}, 1]$ formally reproduces $Z[\Lambda]$ (2.3) (the curvature term can be ignored as it is topological). There is now a great deal of evidence that this identification is correct and that the Euclidean functional integral over the metric can indeed be defined as a sum over triangulations. Much of this evidence comes through the

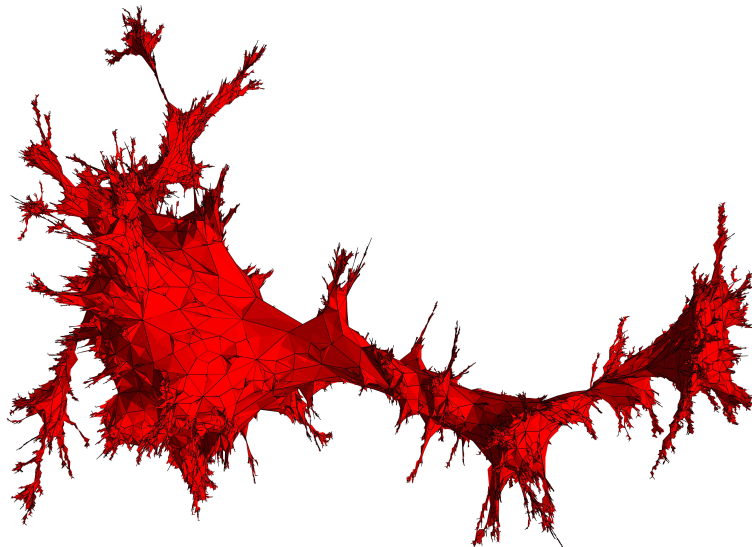


Figure 1. An instance of a large planar map with 30,000 vertices generated by Jérémie Bettinelli [26].

connection between $\mathcal{E}(M)$ and matrix models which was established in [22]; for a modern review see [23].

Each $T \in \mathcal{E}(M)$ is a random planar map. This ensemble has been studied in great detail; one particularly interesting result is that the Hausdorff dimension of very large planar maps is $d_H = 4$ almost surely [24]. Thus such a map must have very non-trivial fractal structure since it is assembled piecewise from two-dimensional triangles (or, more generally, polygons). Figure 1 shows an example of a planar map with a large number of vertices; it is a discrete approximation of the Brownian map [25]. We will return to the characterization of such maps in section 2.5.

2.3 Causal triangulations

The Euclidean triangulations provide a definition of the Euclidean path integral but it is not immediately clear how results in this theory are related to physical quantities in the Lorentzian theory (2.1). This led Ambjørn and Loll [7] to introduce the causal triangulation (CT). The CT triangulates only manifolds that are globally hyperbolic, i.e. they have a time slicing. Consequently the edges in a CT are either time-like or space-like which allows a well-defined Wick rotation between Euclidean and Lorentzian signatures and the notion of causality is automatically incorporated. The model is most often solved in the Euclidean setting but a consistent way to define Lorentzian triangles and angles that satisfy the usual Euclidean additivity conditions exists and was described in [27].

Definition 2.2. *A causal triangulation (CT) C of the disk M is a triangulation where all vertices at a fixed graph distance t from the root form a cycle $S_t(C)$. Its*

height $h(C)$ is the maximum graph distance of the vertices from the root

$$h(C) = \max_{v \in C} \{d(v, v_0)\}.$$

An example is shown in figure 2. It is clear from the definition that each vertex of C at height $t > 0$ has 2 spatial neighbours, several future neighbours σ_v^f and a number of past neighbours σ_v^p such that the total number of neighbours is $\sigma_v = 2 + \sigma_v^f + \sigma_v^p$. The definition is easily extended to annular topology by marking a vertex at height $t = 1$ then deleting the root and the edges attached to it.

Letting $\mathcal{C}(M)$ be the set of distinct causal triangulations of M we define the partition functions

$$W[\tilde{g}, z; t] = \sum_{C \in \mathcal{C}(M): h(C)=t} |S_t(C)| \tilde{g}^{\Delta(C)+1} (z/\tilde{g})^{|S_t(C)|}. \quad (2.8)$$

Note that, in contrast to the Euclidean triangulation case, we now have a natural ‘time’ t which will play an important role in what follows. From the gravitational point of view, W is essentially the discretized path integral for the Euclidean amplitude that a universe evolves from a point to a boundary in time t . There is a critical value $\tilde{g}_c = \frac{1}{2}$ such that the sum in (2.8) converges for $\tilde{g} < \tilde{g}_c$ for all t ; in the limit $\tilde{g} \uparrow \tilde{g}_c$ arbitrarily large triangulations dominate and we recover the path integral for the point-to-boundary amplitude in two-dimensional projectable Horava-Lifshitz gravity [28].

Although the sum to determine $W[\tilde{g}, z; t]$ can be evaluated by elementary means for finite t [7], this gives us little information about the nature of the CTs that contribute at criticality. It was observed in [29] that $\mathcal{C}(M)$ can also be studied by exploiting the existence of a bijection $\beta : \mathcal{C} \rightarrow \mathcal{T}$ with the set of planar rooted trees, see [30] for a recent review.

Definition 2.3. *The bijective map $\beta(C)$ is defined by:*

1. *Mark an edge coming out of v_0 and add a root vertex r to C connected by a single edge to v_0 placed in the face to the right of the marked edge as seen from v_0 .*
2. *Remove all edges in the cycles $S_t(C), \forall t > 0$. i.e. the space-like edges.*
3. *For every $v \in S_t(C)$ where $1 \leq t < h(C)$ remove the rightmost edge of the σ_v^f edges as seen from v .*

The resulting graph T is a tree with a new root vertex r and every vertex from C as shown in figure 2. It is straightforward to show that the inverse map β^{-1} exists. The partition functions W can be rewritten in the tree picture as

$$W[\tilde{g}, z; t] = \sum_{T \in \mathcal{T}: h(T)=t+1} \prod_{v \in V(T) \setminus r} \tilde{g}^{\sigma_v} (z/\tilde{g})^{|S_t(\beta^{-1}(T))|}. \quad (2.9)$$

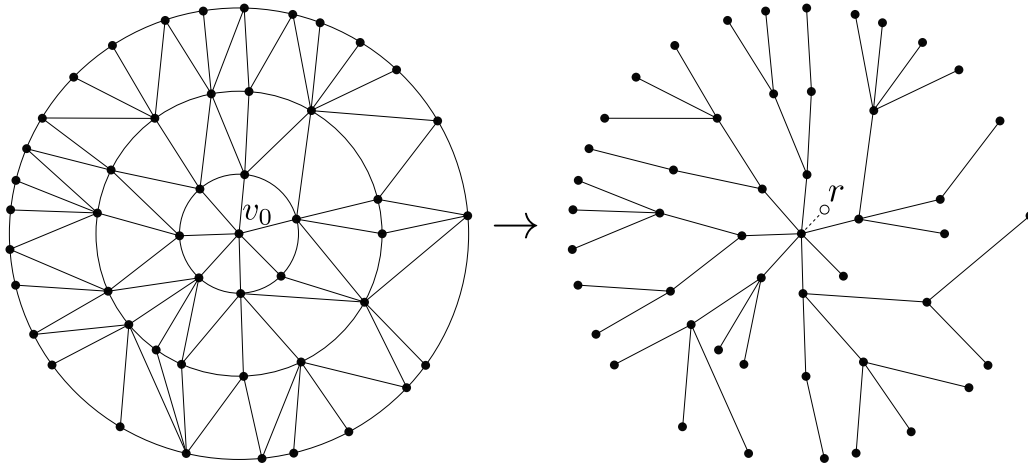


Figure 2. A causal triangulation of height 3, and the action of the map β to its associated tree.

It was shown in [31] that the ensemble (2.9) at criticality, i.e. $\tilde{g} = \frac{1}{2}$, is equivalent to a critical Galton-Watson (GW) process. This is a branching process specified by a set of probabilities $p_n, n = 0, 1, \dots$, called the *offspring probabilities*, having unit mean i.e., $\sum_{n=0}^{\infty} np_n = 1$. The process can be viewed as a tree in which p_n is the probability of a single vertex having n offspring. Recalling that by definition the root vertex has a single offspring with probability one, the probability distribution on finite trees $T \in \mathcal{T}$ is then given by

$$\pi(T) = \prod_{i \in T \setminus r} p_{\sigma_i - 1}. \quad (2.10)$$

Choosing $p_n = 2^{-n-1}$ we see that $\pi(T)$ reproduces the weights in $W[\frac{1}{2}, 1]$; they define the generic random tree ensemble [31]. It is convenient to introduce the generating function for offspring probabilities

$$f(s) = \sum_{n=0}^{\infty} p_n s^n. \quad (2.11)$$

Then $f(1) = 1$, $f'(1) = 1$, and for the generic random tree $f(s) = (2 - s)^{-1}$.

The definition of CTs 2.2 is easily extended to triangulations that have infinite height $h(C) = \infty$ and no boundary; these form the set \mathcal{C}_{∞} and cover the plane. Applying the bijection β 2.3 to $C \in \mathcal{C}_{\infty}$ then yields an infinite tree $T \in \mathcal{T}_{\infty}$. It was shown in [30] that one can extend the probability distribution $\pi(T)$ on finite trees to a measure $\nu(T)$ on $T \in \mathcal{T}_{\infty}$. Provided only that $f''(1) < \infty$, $\nu(T)$ is concentrated on single spine trees [30, 32]. The spine is a sequence of vertices r, s_1, s_2, \dots starting at the root and going off to infinity with no backtracking. Attached to each spine vertex, with probability p'_n generated by $sf'(s)$, is a set of n finite trees with vertices

distributed according to $f(s)$. The ensemble defined by the set of triangulations \mathcal{C}_∞ and the probability measure on them $\mu(C) = \nu(\beta^{-1}(C))$ is called the Uniform Infinite Causal Triangulation (UIC T).

2.4 Coupling matter

To implement the matter action S_m (2.3) in the discretized picture we introduce new degrees of freedom that live on the vertices of the graphs G in the ensemble. In this paper we work specifically with Ising spins but the construction is easily generalised, in particular to the random height models. On each vertex $v \in V(G)$ lives a spin that takes values in $\{+1, -1\}$, and spins on vertices that share an edge $e \in E(G)$ interact with a coupling strength J_e . The spin partition function on G is given by the sum over all spin configurations

$$Z_G[\{J\}_G] = \sum_{\{\sigma \in \{+1, -1\}^{V(G)}\}} \exp \left(\sum_{e=\langle x, y \rangle \in E(G)} J_e \sigma_x \sigma_y \right). \quad (2.12)$$

From now on we will assume that for the \mathcal{E} ensemble $J_e = J, \forall e$, and that for the \mathcal{C} ensemble $J_e = J_1$ for all space-like edges and $J_e = J_2$, for all time-like edges. The discretised Euclidean and CT path integrals for the disk corresponding to (2.3) then take the form

$$W_{\mathcal{G}} = \sum_{G \in \mathcal{G}} \tilde{g}^{\Delta(G)} z^{|\partial G|} Z_G[J_{\mathcal{G}}], \quad (2.13)$$

where \mathcal{G} is chosen to be respectively \mathcal{E} or \mathcal{C} . We refer to the systems described by $W_{\mathcal{G}}$ as *annealed* models.

In statistical mechanics language $W_{\mathcal{G}}$ is the grand canonical partition function. For given $J_{\mathcal{G}}$ the sum is convergent for $\tilde{g} < \tilde{g}_c(J_{\mathcal{G}})$. In the coupling strength region $J_{\mathcal{G}} \in \mathcal{A}$ where $\tilde{g}_c(J_{\mathcal{G}})$ is analytic, the limit $\tilde{g} \uparrow \tilde{g}_c(J_{\mathcal{G}})$ describes the same purely gravitational physics as the partition function without matter degrees of freedom. On the other hand, in the region $J_{\mathcal{G}} = J_{\mathcal{G}}^* \in \partial \mathcal{A}$ where $\tilde{g}_c(J_{\mathcal{G}})$ is not analytic the spins become critical on the very large graphs in the sum – they magnetize in the case of the Ising model. The limit $\tilde{g} \uparrow \tilde{g}_c(J_{\mathcal{G}}^*)$ then describes a continuum theory of gravity interacting with matter (central charge $c = \frac{1}{2}$ conformal matter in the Ising case). The matrix model solution [5, 6] for $W_{\mathcal{E}}$ shows that the Ising scaling exponents are shifted away from their regular \mathbb{Z}^2 lattice values; they are related to each other by the KPZ formula which can be understood in a number of ways as is discussed below in section 2.5. Numerical simulations and series expansions for \mathcal{C} [8] strongly suggest that the scaling exponents for Ising spins are not shifted from their regular lattice values, but no exact solution for $W_{\mathcal{C}}$ is known.

An alternative formulation of the CT interacting with matter is provided by working in the canonical ensemble with the graphs $C \in \mathcal{C}_\infty$. In principle we have

a new measure $\mu_J(C)$ that reflects the relative weight of the Ising partition function $Z_C(J)$ on different graphs. As critical behaviour of the spins only occurs on very large graphs we might expect $\mu_J(C)$ to capture the same physics as the grand canonical partition function W_C ; unfortunately $\mu_J(C)$ is yet to be constructed. An intermediate step is to analyse the critical properties of an Ising spin system living on a triangulation sampled from the UICCT ensemble according to the measure μ , which we call the *quenched* model. In [29] it was shown that at small J this system has a unique Gibbs measure (corresponding to unmagnetized spins), while at large J (at least) two Gibbs measures co-exist (corresponding to two possible magnetised states); furthermore it was shown that almost surely (i.e. with probability one in the measure μ) the critical temperature is the same for any C . The main purpose of this paper is to show that *if* this critical point leads to a scaling limit, *then* the corresponding field theory must contain operators with the same scaling exponents as those appearing in the scaling limit of the flat lattice Ising model.

2.5 Liouville gravity à la Duplantier-Sheffield

The Liouville gravity approach to computing the gravitational path integral was introduced by Polyakov [33]. We outline the basic features here (see [34, 35] for a detailed review of the topic). Any 2D metric can be written as $g = e^\phi \hat{g}$, where ϕ is a dynamical degree of freedom and \hat{g} is a fixed background metric which can always be taken to be flat Euclidean space, assuming a suitable topology. The Euclidean Einstein-Hilbert action reduces to the Liouville action for the scalar field ϕ given by

$$S_L = \int d^2z \sqrt{\hat{g}} (\hat{g}^{ab} \partial_a \phi \partial_b \phi + Q \hat{R} \phi + \Lambda e^{\gamma \phi}) + S_{CFT}. \quad (2.14)$$

Here \hat{R} is the Ricci curvature associated with \hat{g} , Λ is the cosmological constant and S_{CFT} is the action of some conformal matter with central charge c . The requirement that there is no conformal anomaly then determines $Q = \frac{2}{\gamma} + \frac{\gamma}{2}$, where γ is given by

$$\gamma = \frac{1}{\sqrt{6}} (\sqrt{25 - c} - \sqrt{1 - c}). \quad (2.15)$$

For example, pure gravity ($c = 0$) corresponds to $\gamma = \sqrt{8/3}$ whereas the scaling limit of the Ising model ($c = \frac{1}{2}$) corresponds to $\gamma = \sqrt{3}$.

The Liouville path integral for pure gravity, taking background metric $\hat{g}_{ab} = \delta_{ab}$, is written formally as

$$Z[\Lambda] = \int \mathcal{D}\phi e^{-\int d^2z \partial_a \phi \partial^a \phi + \Lambda e^{\gamma \phi}}. \quad (2.16)$$

To make rigorous sense of (2.16) we must define the measure on ϕ . In the probabilistic approach to QFT, the idea is that the term $e^{-\int d^2z \partial_a \phi \partial^a \phi}$ is proportional to a Gaussian measure on the space of functions $\phi : D \rightarrow \mathbb{R}$ with Dirichlet boundary conditions

where $D \subset \mathbb{R}^2$ [36]. This ensemble is called the *Gaussian free field* (GFF); it is a generalisation of Brownian motion to higher dimensions and is defined as follows.

Definition 2.4. Let $D \subset \mathbb{R}^d$ be some domain and define the inner product on functions $f : D \rightarrow \mathbb{R}$ as

$$\langle f, g \rangle_{\nabla} := \frac{1}{2\pi} \int_D \nabla f \cdot \nabla g d^d z, \quad (2.17)$$

and associated norm

$$\|h\|_{\nabla}^2 := \frac{1}{2\pi} \int_D \nabla h \cdot \nabla h d^d z. \quad (2.18)$$

The GFF is defined to be the measure whose probability density is given by

$$\rho(h) = \text{const.} \exp\left(-\frac{1}{2}\|h\|_{\nabla}^2\right). \quad (2.19)$$

The density $\rho(h)$ is nothing but the path integral measure for the massless free boson with Dirichlet boundary conditions. Hence the formal path integral (2.16) is defined rigorously as

$$\int \mathcal{D}\phi e^{-\int d^2 z \partial_a \phi \partial^a \phi + \Lambda e^{\gamma \phi}} = \mathbb{E}[e^{-\int d^2 z \Lambda e^{\gamma \phi}}], \quad (2.20)$$

where the expectation is over the GFF measure.

In this formulation of Liouville gravity, the cosmological constant couples to the random area

$$A = \int e^{\gamma \phi} d^2 z, \quad (2.21)$$

generated by the GFF ϕ . On the common base space $[0, 1]^2$ there are then two measures:

- The Lebesgue measure on $[0, 1]^2$, $d^2 z$;
- The random measure $d\mu_{\gamma} = e^{\gamma \phi} d^2 z$, where ϕ is a GFF.

To visualize the random measure μ_{γ} , choose $\delta \in (0, 1)$ and, starting with the base space $[0, 1]^2$, iteratively divide squares into four quadrants to obtain the set of largest square regions $S_i \subset [0, 1]^2$ such that $\mu_{\gamma}(S_i) \leq \delta$. This defines the *dyadic square decomposition* where each square has roughly the same quantum area δ . The decomposition is shown in figure 3 for a particular instance of the GFF. It is clear that different matter on the background, which changes the value of γ by (2.15), determines the strength of the fluctuations.

Duplantier and Sheffield [13] observed that a subset $K \subset [0, 1]^2$ can be measured by using either the Lebesgue measure or the random measure. The random measure with fixed $\phi = 0$, *i.e.* no fluctuations in the 2D metric, is simply the Lebesgue measure, so the relationship between the two results characterises the effect of gravity on K . To make this relationship precise first define two kinds of balls:

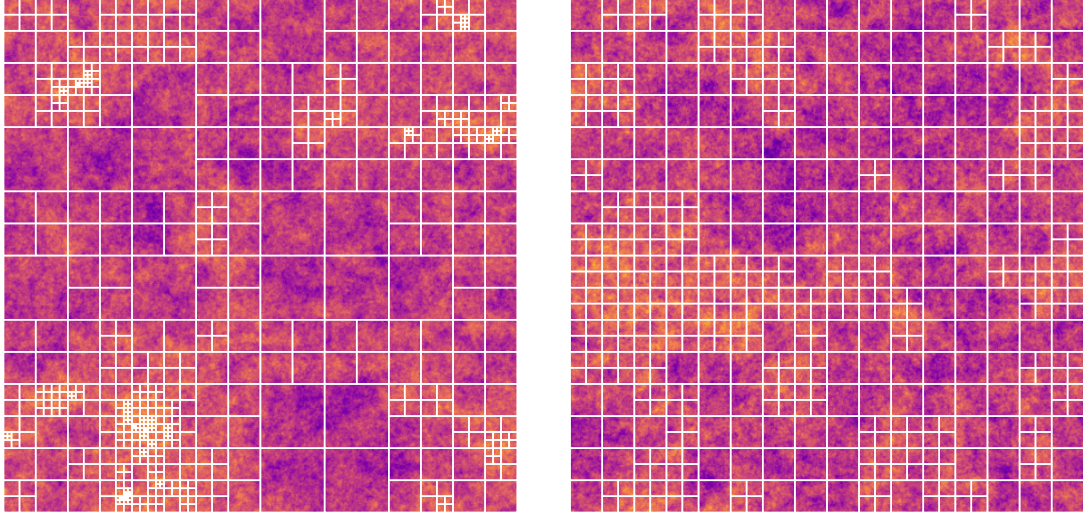


Figure 3. A dyadic decomposition of $e^{\gamma\phi}$ with $\gamma = 2$ (left) and $\gamma = 0.5$ (right)

Definition 2.5 (Euclidean and quantum balls). For all $z \in [0, 1]^2$:

- $B_\epsilon(z)$ is the Euclidean ball of radius ϵ centred on z ;
- $B^\delta(z)$ is the quantum ball centred on z and of quantum area δ i.e. It is the Euclidean ball $B_\tau(z)$ with $\tau := \sup\{r \geq 0, \mu_\gamma(B_r(z)) \leq \delta\}$.

We can then define two different scaling exponents for some fixed subset $K \subset [0, 1]^2$:

Definition 2.6 (Euclidean and quantum scaling).

- The **Euclidean scaling exponent** $x = x(K)$ is defined as

$$x(K) := \lim_{\epsilon \rightarrow 0} \frac{\log \mathbb{P}[B_\epsilon(z) \cap K \neq \emptyset]}{\log \epsilon^2}, \quad (2.22)$$

where z is sampled according to, and the probability \mathbb{P} computed in, the Lebesgue measure;

- The **quantum scaling exponent** $\Delta = \Delta(K)$ is defined as

$$\Delta(K) := \lim_{\delta \rightarrow 0} \frac{\log \mathbb{E}[\mu_\gamma[B^\delta(z) \cap K \neq \emptyset]]}{\log \delta}, \quad (2.23)$$

where z is sampled according to, and the expectation \mathbb{E} computed in, the random measure μ_γ .

The main result of Duplantier-Sheffield [13] is the derivation of the *Knizhnik-Polyakov-Zamolodchikov* (KPZ) formula [2] that relates these two scaling dimensions by

$$x = \frac{\gamma^2}{4} \Delta^2 + \left(1 - \frac{\gamma^2}{4}\right) \Delta. \quad (2.24)$$

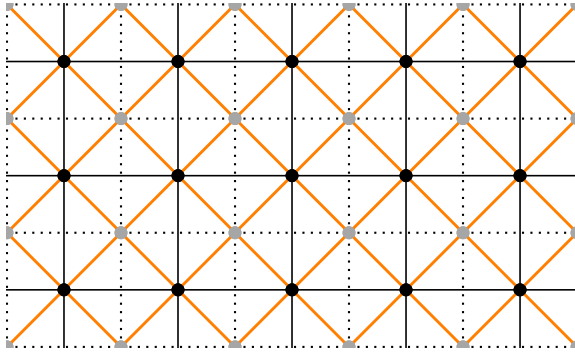


Figure 4. The graph \tilde{G} (orange) formed from the original square lattice (black), and its dual (gray, dashed).

Taking the Ising model as an example, we have $\gamma = \sqrt{3}$ and 2 primary fields ε, σ with scaling dimensions $x_\varepsilon = 1/2, x_\sigma = 1/16$. Using (2.24) we find that the quantum scaling dimensions take the shifted values

$$\Delta_\varepsilon = 2/3, \quad \Delta_\sigma = 1/6.$$

These are in agreement with the matrix model calculations of Kazakov et al [5, 6].

3 The Ising model and topological defects

The exact microscopic connection between topological defects in the two-dimensional Ising model and the corresponding fusion category was elucidated in [12], and then extended to general height models in [37]. In this section we review the formalism for the Ising model given in [12], and describe in detail how it can be applied to CT graphs of disk or annulus topology.

3.1 The Ising model in the plaquette formalism

Consider the Ising model with partition function $Z_G[\{J\}_G]$ (2.12) defined on a planar graph G . Now construct a new graph \tilde{G} formed by combining G with its dual G^* as follows: start with G and G^* overlaying each other, then join each G vertex to the nearest G^* vertices without crossing any original or dual edges, and finally remove the original and dual edges. See figure 4 for the case when G is a square lattice. The graph \tilde{G} is formed of quadrilateral faces with opposite vertices belonging to the original or dual map. We call these quadrilateral faces *plaquettes*. It is important to note that the spins exist either on G or on G^* , but not both. Therefore, each plaquette only has 2 spins. Each plaquette represents an edge between spins on the original lattice.

If G is a CT, we have two types of plaquettes in \tilde{G} , *horizontal* and *vertical* as shown in figure 5. By assigning weights to each plaquette we can rewrite the partition function as a product of these weights. First, we define u_H and u_V via

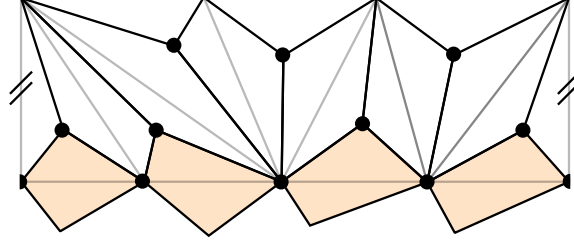


Figure 5. Horizontal (orange) and vertical plaquettes for a single CDT strip where the dots show the location of the weights d_v .

$$e^{2J_V} = \cot u_V, \quad e^{2J_H} = \cot\left(\frac{\pi}{4} - u_H\right). \quad (3.1)$$

where J_H and J_V are the couplings for horizontal and vertical edges respectively. It is useful in the context of defects to re-define the partition function to include a vertex factor d_v [12]

$$d_v = \begin{cases} 1 & \text{if } v \text{ has a spin} \\ \sqrt{2} & \text{if } v \text{ is empty.} \end{cases} \quad (3.2)$$

We assign these weights to the plaquettes by splitting them between the left and right vertices. Since the vertical plaquettes only have spins on the top and bottom positions this gives an additional $\sqrt{2}$ factor. Horizontal plaquettes have spins on the left and right positions so the additional factor from the weights is 1. We then define the weights for each plaquette

$$W_j^V(u_V) \equiv \begin{array}{c} a \\ \diamond \\ b \end{array} = \sqrt{2} (\cos u_V \delta_{ab} + \sin u_V \sigma_{ab}^x) = \begin{cases} \cos u_V & a = b \\ \sin u_V & a \neq b \end{cases}$$

$$W_j^H(u_H) \equiv a \begin{array}{c} \diamond \\ b \end{array} = \frac{1}{\sqrt{2}} (\cos u_H + (-1)^{a+b} \sin u_H) = \begin{cases} \cos(\frac{\pi}{4} - u_H) & a = b \\ \sin(\frac{\pi}{4} - u_H) & a \neq b \end{cases} \quad (3.3)$$

where the labels are related to the spins by $\sigma = (-1)^a$. The partition function is now a product of plaquettes

$$Z_G[J_V, J_H] = \sum_{\{\sigma\}} \prod_{p \in \mathcal{P}_{\tilde{G}}} a_p \begin{array}{c} b_p \\ \diamond \\ d_p \end{array} c_p, \quad (3.4)$$

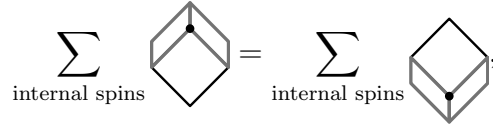
where $\mathcal{P}_{\tilde{G}}$ denotes the set of plaquettes in \tilde{G} .

3.2 The spin-flip defect


One can define an Ising model in the presence of a spin defect. A spin defect is a one-dimensional object that bisects a sequence of edges in the original lattice and swaps the couplings $J \rightarrow -J$, turning the interaction from ferromagnetic to anti-ferromagnetic and vice versa. We can implement this defect in the plaquette formalism by cutting a path along \tilde{G} and splitting the lattice in two – making a copy of every spin along the cut. We then insert a sequence of parallelograms which have a factor proportional to the Pauli matrix σ^x , enforcing that the spins on each side of the parallelogram are opposite. The weight of the parallelogram is

$$\boxed{a}_b = 2^{-1/4} [\sigma^x]_{a,b} = \begin{cases} 0 & a = b \\ 2^{-1/4} & a \neq b. \end{cases} \quad (3.5)$$

With this definition, we can compute the effect of local manipulations and show that the spin defect can be moved around without changing the partition function i.e. it is a *topological defect*. In particular, for a defect to be topological, we must show the following defect commutation relations

$$\sum_{\text{internal spins}} \text{diag}_1 = \sum_{\text{internal spins}} \text{diag}_2, \quad (3.6)$$


along with this diagram rotated by 90 degrees. We must also show

$$\sum_{\text{internal spins}} \text{diag}_3 = \text{diag}_4, \quad (3.7)$$


where the dots represent the weights d_v . These two relations for a general defect (represented by the gray parallelograms) show that you can move the defect line around the lattice without changing the partition function. It was shown by Aasen et al. [12] that with the definition of the spin defect in (3.5), these defect commutation relations are indeed satisfied.

3.3 The duality defect

The Ising model has one more non-trivial defect which implements the Kramers-Wannier duality of the Ising model [12]. The Kramers-Wannier duality replaces spins on the lattice with spins on the dual lattice. Hence, a duality defect must stitch together spins on G on one side with spins on G^* on the other – this is where the \tilde{G} picture comes into its own. We define the parallelogram for the duality defect as

$$\boxed{a}_b = 2^{-1/2} (-1)^{ab}. \quad (3.8)$$

It was shown in [12] that this satisfies the defect commutation relations (3.6 - 3.7) proving that it is a topological defect. An important difference between the spin defect and the duality defect is the position of the spins. The spins are on opposite sides of the parallelogram for the duality defect. This has the effect of changing the plaquettes from vertical to horizontal and vice versa i.e. $W^H(u_H) \rightarrow W^V(u_H)$ and $W^V(u_V) \rightarrow W^H(u_V)$.

3.4 The Ising fusion category

The microscopic calculations shown in the previous sections and computed in detail in [12] allow us to forget about individual spins/plaquettes and instead deal directly with these extended defect lines. These defect lines form the structure of a *fusion category* that we will detail in this section. For completeness, we specify all the data of the Ising fusion category. We will not give a rigorous definition of fusion categories here but we will simply state the objects and formal manipulations one is allowed to perform. Any fusion category has a finite set of objects L , which in the case of the Ising category are the duality field σ , the spin field ψ and the identity $\mathbf{1}$. Each object is represented diagrammatically as a line in a graph. These objects satisfy an algebra, which in general, can be written as

$$a \times b = \sum_c N_{ab}^c c, \quad (3.9)$$

where $a, b, c \in \{\mathbf{1}, \psi, \sigma\}$ and $N_{ab}^c \in \mathbb{N}$. The Ising algebra is

$$\psi \times \psi = \mathbf{1}; \quad \psi \times \sigma = \sigma \times \psi = \sigma; \quad \sigma \times \sigma = \mathbf{1} + \psi. \quad (3.10)$$

The vertex factors d_a in (3.2) are called the *Frobenius-Perron dimensions* or *quantum dimensions* and are defined as the maximal eigenvalues of the algebra coefficient matrix $[N_a]_b^c$. Again, for the Ising category these are $d_\psi = d_{\mathbf{1}} = 1$ and $d_\sigma = \sqrt{2}$. The final piece of data in a fusion category are the *F-symbols*. These dictate the diagrammatic rules of the objects in L called *F-moves*. A general *F-move* takes the form

$$\begin{array}{c}
 a \quad b \quad c \\
 \diagdown \quad \diagup \quad / \\
 \text{---} X \text{---} \\
 | \\
 d
 \end{array}
 = \sum_Y [F_d^{abc}]_{XY}
 \begin{array}{c}
 a \quad b \quad c \\
 \diagdown \quad \diagup \quad / \\
 \text{---} Y \text{---} \\
 | \\
 d
 \end{array}
 \quad (3.11)$$

where the numbers $[F_d^{abc}]_{XY} \in \mathbb{R}$ are the *F-symbols*. These are not independent free parameters, they must satisfy a number of self-consistency conditions [37]. One such

solution for the Ising category has the following non-trivial F -symbols:

$$\begin{aligned}
[F_\sigma^{\sigma\sigma\sigma}]_{\mathbb{1}\mathbb{1}} &= [F_\sigma^{\sigma\sigma\sigma}]_{\mathbb{1}\psi} = [F_\sigma^{\sigma\sigma\sigma}]_{\psi\mathbb{1}} = \frac{1}{\sqrt{2}}, \\
[F_\sigma^{\sigma\sigma\sigma}]_{\psi\psi} &= -\frac{1}{\sqrt{2}}, \\
[F_\psi^{\sigma\psi\sigma}]_{\sigma\sigma} &= [F_\sigma^{\psi\sigma\psi}]_{\sigma\sigma} = -1.
\end{aligned}
\tag{3.12}$$

Any vertex that would imply the fusion of objects not allowed by the fusion algebra has a vanishing F -symbol. The remaining non-zero F -symbols in the Ising category are 1 if allowed by the fusion algebra. We can compute an arbitrary planar fusion diagram using (3.11–3.12) and the following rules:

$$\begin{aligned}
\bigcirc^a &= d_a, & \begin{array}{c} c \\ | \\ \bigcirc \\ | \\ a \end{array} b &= \delta_{ac} \sqrt{\frac{d_b d_{b'}}{d_a}}.
\end{aligned}
\tag{3.13}$$

In Figure 6 we show some examples of the application of the F -moves to the manipulation of topological defects.

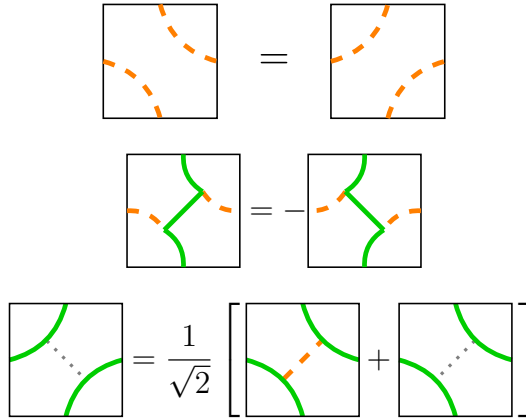


Figure 6. Non-trivial F -moves in the Ising fusion category. All of these moves are local and require no particular topology. The green solid line is the duality defect σ , the orange dashed line is the spin defect ψ and the thin dotted line is the identity $\mathbb{1}$ (which is often omitted in the diagrams).

This association between topological defects in lattice models and fusion categories was fully established in [37] where it is shown that the construction extends to general height models.

3.5 Dehn twist operators on the lattice

A Dehn twist is an operation that cuts out a concentric circle at some finite distance from the origin, twists one half by a full revolution and glues the two halves back

together at the end. We show that operators that implement a Dehn twist can be constructed on a CT similar to those constructed in [12].

Consider the partition function $Z(C)$ where $C \in \mathcal{C}_\infty \setminus D$, where D is a topological disk and hence C is a punctured plane. This is a natural space to consider for a CT because we often think of an initial boundary evolving radially. The partition function is best represented by the diagram

$$Z(C) = \text{Diagram} \quad (3.14)$$

where \mathcal{P}_∞ is a path from a marked point on the inner boundary to the infinite boundary. Now consider the addition of an Ising defect that starts at some other (not necessarily different) marked point on the boundary and extends to infinity, crossing \mathcal{P}_∞ n times. We call this partition function $Z_n^\phi(C)$ where $\phi = \mathbb{1}, \psi, \sigma$ and we represent this diagrammatically by

$$Z_n^\phi(C) = \text{Diagram} \quad (3.15)$$

We show in Appendix A that the defect can be pinned to the inner boundary by an appropriate choice of boundary conditions which prevents the defect from unravelling.

There is a second way of looking at this construction – in a transfer matrix formalism. For any height t we define the spin configuration $|\{h_i^t\}\rangle$ as a vector in a Hilbert space \mathcal{H}_ϕ . The transfer matrix evolves a state $|\{h_i^t\}\rangle$ to a state $|\{h_i^{t+1}\}\rangle$. There is a subtle distinction here: unlike a regular square lattice, each height in a CT does not generally have the same number of spins. While this complicates writing a compact expression for the transfer matrix, this issue is purely aesthetic. We have demonstrated that local manipulations can be performed that satisfy (3.6–3.7), allowing us to move any defect (that does not extend to the infinite boundary) to a chosen height t – this is where we will define all of the Dehn twist operators.

Lemma 3.1 (Dehn twist operators). *For all $C \in \mathcal{C}_\infty \setminus D$, each defect $\phi = \psi, \sigma$ and every height t there is an operator \mathbf{T}_ϕ acting on the Hilbert space \mathcal{H}_ϕ at height t satisfying the relations*

1. $\mathbf{T}_\psi^2 - \mathbb{1}_\psi = 0$,
2. $\mathbf{T}_\sigma^4 - \sqrt{2}\mathbf{T}_\sigma^2 + \mathbb{1}_\sigma = 0$,

where the operators $\mathbb{1}_\phi$ act as the identity in the presence of a vertical defect ϕ , i.e. $\mathbb{1}_\phi |\{h_i\}\rangle = |\{h_i\}\rangle$.

Proof. Consider the first case, where we have a spin defect that runs from the inner boundary out to infinity without crossing \mathcal{P}_∞ represented by the diagram

$$Z_0^\psi(C) = \text{Diagram} \quad (3.16)$$

We choose some fixed height t and define the operators $\mathbb{1}_\psi$ and \mathbf{T}_ψ by the following plaquette diagrams

$$\mathbb{1}_\psi = \text{Diagram} \quad (3.17)$$

$$\mathbf{T}_\psi = \text{Diagram} \quad (3.18)$$

It turns out that the operator that implements the Dehn twist with a vertical spin defect is simply a horizontal spin defect \mathcal{D}_ψ with the two triangle junctions that allow defect lines to join in the plaquette formalism [12]. Applying local moves in the partition function picture one can move the plaquettes:

$$\text{Diagram 1} = \text{Diagram 2} = \text{Diagram 3}, \quad (3.19)$$

clearly implementing the Dehn twist as desired. Applying \mathbf{T}_ψ^2 at height t , we can use local moves to move one insertion of \mathbf{T}_ψ to a height $t' > t$ and apply F -moves to the defect lines:

$$Z_2^\psi(C) = \text{Diagram 1} = \text{Diagram 2} = \text{Diagram 3} = Z_0^\psi(C), \quad (3.20)$$

or in terms of operators $\mathbf{T}_\psi^2 |\{h_i\}\rangle = \mathbb{1}_\psi |\{h_i\}\rangle$.

The calculation for the duality defect follows the same lines but with some added technical details. Consider a single duality defect that starts from the inner boundary

and extends to infinity without wrapping around the centre shown diagrammatically by

$$Z_0^\sigma(C) = \text{[Diagram: A dashed circle with a central dot and a green line segment extending from the center to the boundary.]} \quad (3.21)$$

There is an additional subtlety in the duality case compared to the previous spin one. The duality defect interfaces between spins living on the vertices of C and spins living on the vertices of C^* . Due to the topology of the space we are considering, there must be another boundary where C and C^* meet again – this is the wall. We choose to place the wall along \mathcal{P}_∞ for convenience. Crucially, we show in Appendix B that the wall does not pose a problem in any manipulations that follow.

As before, we define an identity operator and an operator \mathbf{T}_σ that act on the spins at height t in terms of the plaquettes

$$\mathbf{1}_\sigma = \text{[Diagram: A zigzag chain of vertices with a green line segment labeled \sigma and a shaded region labeled wall.]} \quad (3.22)$$

$$\mathbf{T}_\sigma = \text{[Diagram: A zigzag chain of vertices with a green line segment labeled \sigma and a shaded region labeled wall.]} \quad (3.23)$$

where the appropriate wall plaquettes are included. The operators $\mathbf{1}_\sigma$ and \mathbf{T}_σ can also be defined on the slice where the spins are on the other diagonals of the duality plaquettes. This gives us two isomorphic Hilbert spaces \mathcal{H}_σ and $\hat{\mathcal{H}}_\sigma$. Currently, \mathbf{T}_σ takes \mathcal{H}_σ to $\hat{\mathcal{H}}_\sigma$ and vice-versa. Instead we can unify this into one operator that acts on $\mathcal{H}_\sigma \oplus \hat{\mathcal{H}}_\sigma$ [12].

Applying \mathbf{T}_σ^2 at height t and applying local topological moves, we can use the partition function picture and F -moves to compute the result:

$$\begin{aligned} Z_2^\sigma(C) &= \text{[Diagram: A dashed circle with a green spiral line inside.]} = \frac{1}{\sqrt{2}} \left[\text{[Diagram: A dashed circle with a green spiral line and a small orange dot.]} + \text{[Diagram: A dashed circle with a green spiral line.]} \right], \\ &= \frac{1}{\sqrt{2}} \left[\text{[Diagram: A dashed circle with a green line segment and an orange dashed circle.]} + \text{[Diagram: A dashed circle with a green line segment and a dotted circle.]} \right], \end{aligned}$$

where the details of how the defects pass through the wall can be found in Appendix B. In terms of the operators:

$$\mathbf{T}_\sigma^2 = \frac{1}{\sqrt{2}}(\psi_\sigma + \mathbb{1}_\sigma), \quad (3.24)$$

$$\mathbf{T}_\sigma^4 = \frac{1}{2}(\psi_\sigma + \mathbb{1}_\sigma)^2 = \frac{1}{2}(\mathbb{1}_\sigma + 2\psi_\sigma + \psi_\sigma^2), \quad (3.25)$$

where ψ_σ is an operator made of horizontal spin plaquettes in the presence of a vertical duality defect – we omit an explicit diagram for the sake of brevity. It remains to calculate ψ_σ^2 , which is most easily done diagrammatically with the use of F -moves:

or in terms of operators $\psi_\sigma^2 = -\mathbb{1}_\sigma$, which gives us an algebraic equation for \mathbf{T}_σ :

$$\mathbf{T}_\sigma^4 = \sqrt{2}\mathbf{T}_\sigma^2 - \mathbb{1}_\sigma. \quad (3.26)$$

□

Corollary 3.2 (Eigenvalues of Dehn twist operators). *The eigenvalues of the operators \mathbf{T}_ψ and \mathbf{T}_σ are given by*

- $\mathbf{T}_\psi : \lambda = \pm 1$
- $\mathbf{T}_\sigma : \lambda = e^{2\pi i/16}, e^{-2\pi i/16}, e^{-2\pi i \cdot 7/16}, e^{2\pi i \cdot 7/16}$

Proof. Both relations follow directly by turning the operator equations in Lemma 3.1 into eigenvalue equations. In the spin defect case, this becomes $\lambda^2 = 1$. In the duality defect case, we have $\lambda^4 - \sqrt{2}\lambda^2 + 1 = 0$. □

The Dehn twist is a topological construction, meaning any results from the lattice persist in a continuum limit given that it is possible to construct a Dehn twist in the continuum. Vertical defects create twisted boundary conditions and in the continuum CFT description, boundary operators are in bijection to the primary fields [38]. Hence, by constructing a topological argument on the lattice, we can make claims about the scaling dimensions of fields in the continuum. The aim is to use the results of Corollary 3.2 and compare them to the known form of the operator in the continuum given by $e^{2\pi i(L_0 - \bar{L}_0)}$. Before we can do this, we must first prove that it is possible to construct a Dehn twist on continuum CTs, which we do in the following section.

4 Stochastic formulation of CDT

We derive a stochastic differential equation for the length of the spatial slice at time t starting from the discrete Galton-Watson process as an alternative to the results in [39, 40]. We then show how this generates a random measure on some base space in an exact analogy to the Liouville gravity picture.

4.1 The Lamperti-Ney Process

Theorem 4.1 (Lamperti-Ney Process). *Let $L(t)$ be the length of the spatial slice at time t . Then $L(t)$ satisfies the Itô integral equation*

$$L(t) = L(0) + \int_0^t \sqrt{f''(1)L(s)} dW(s) + \int_0^t f''(1) ds, \quad (4.1)$$

or equivalently, the stochastic differential equation

$$dL(t) = \sqrt{f''(1)L(t)} dW(t) + f''(1) dt, \quad (4.2)$$

where $f(s)$ is the generating function of the GW process. We call $L(t)$ a Lamperti-Ney Process (LNP) since it was first discovered by them [39].

Before we prove this we need to introduce some definitions and prove some lemmas. We showed that the ensemble of infinite CTs is in bijection to critical GW trees conditioned to survive forever. The number of points at height $k + 1$, η_{k+1} is given by

$$\eta_{k+1} = \eta_k + \sum_{j=1}^{\eta_k - 1} Z_j + Z_0, \quad (4.3)$$

where $Z_j = Y_j - 1$ and $\{Y_j\}$ are i.i.d. random variables whose distribution is given by the generating function $f(s)$, i.e. they are the random variables whose value is the number of offspring of a point on the spatial slice. Similarly, $Z_0 = Y_0 - 1$ where Y_0 is the number of offspring of the special vertex on the infinite spine, which is distributed according to $sf'(s)$ [30]. We list the following results for future reference:

$$\begin{aligned} \mathbb{E}Z_k &= 0, \\ \mathbb{E}Z_0 &= f''(1), \\ \mathbb{E}[Z_k^2] &= f''(1). \end{aligned} \quad (4.4)$$

We define the re-scaled process $L_k^n := \eta_k/n$, where n is some integer which we will take to infinity at the end. Rewriting (4.3) in terms of L_k^n becomes

$$L_{k+1}^n = L_k^n + \frac{1}{n} \left(\sum_{j=1}^{nL_k^n - 1} Z_j + Z_0 \right) \quad (4.5)$$

Lemma 4.2. *Define*

$$\xi_{k+1}^n = \frac{1}{\sqrt{nL_k^n}} \left[\sum_{j=1}^{nL_k^n-1} Z_j + Z_0 - \mathbb{E}Z_0 \right]. \quad (4.6)$$

Then $W_n(t) := \frac{1}{\sqrt{n}} \sum_{k=1}^{\lfloor nt \rfloor} \xi_k^n$ is a Martingale and $W_n(t) \Rightarrow W(f''(1)t) = \sqrt{f''(1)}W(t)$ where W is a standard Brownian motion. The convergence (\Rightarrow) is in distribution.

Proof. From Ethier & Kurtz [41] $W_n(t)$ is a Martingale if $\mathbb{E}[\xi_{k+1}^n | \mathcal{F}_k^n] = 0$, where \mathcal{F}_k^n is the filtration at k . This is true since given L_k , ξ_{k+1}^n is a sum of random variables with mean 0. To show convergence in distribution as it is sufficient to show

$$\frac{1}{n} \sum_{k=1}^{\lfloor nt \rfloor} (\xi_k^n)^2 \rightarrow f''(1)t$$

in probability as $n \rightarrow \infty$.

$$\begin{aligned} \frac{1}{n} \sum_{k=1}^{\lfloor nt \rfloor} (\xi_k^n)^2 &= \frac{1}{n} \sum_{k=1}^{\lfloor nt \rfloor} \frac{1}{nL_k^n} \left(\sum_{i=1}^{nL_k^n-1} Z_i + Z_0 - \mathbb{E}[Z_0] \right)^2 \\ &= \frac{1}{n} \sum_{k=1}^{\lfloor nt \rfloor} \frac{1}{nL_k^n} \sum_{i=0}^{nL_k^n-1} Z_i^2 + \dots \\ &\rightarrow f''(1)t \end{aligned} \quad (4.7)$$

where in the second to last line, we ignore cross terms (because the Z_i are independent) and the terms which will surely vanish as $n \rightarrow \infty$. In the final line, we used the law of large numbers and $\mathbb{E}[Z_i^2] = f''(1)$. \square

Proof of Theorem 4.1. We can re-write equation 4.5 in terms of ξ_k .

$$L_{k+1}^n = L_k^n + \frac{\sqrt{L_k^n}}{\sqrt{n}} \xi_{k+1}^n + \frac{\mathbb{E}[Z_0]}{n} \quad (4.8)$$

Following Kurtz and Protter [42] we define $L_n(t) := L_{\lfloor nt \rfloor}^n$, $W_n(t) := \frac{1}{\sqrt{n}} \sum_{k=1}^{\lfloor nt \rfloor} \xi_k^n$ and $V_n(t) := \lfloor nt \rfloor / n$ where $\lfloor nt \rfloor$ denotes the nearest integer to nt . It then follows that

$$L_n(t) = L_n(0) + \int_0^t \sqrt{L_n(s)} dW_n(s) + \int_0^t \mathbb{E}[Z_0] dV_n(s). \quad (4.9)$$

By Lemma 4.2 we know $W_n(t) \Rightarrow \sqrt{f''(1)}W(t)$ where W is a standard Wiener process and $V_n(t) \Rightarrow V(t) = t$. Kurtz and Protter [42] showed in general that for any process of this form, $L_n(t) \Rightarrow L(t)$ where $L(t)$ satisfies the integral stochastic equation

$$L(t) = L(0) + \int_0^t \sqrt{f''(1)L(s)} dW(s) + \int_0^t \mathbb{E}[Z_0] ds \quad (4.10)$$

or in differential form

$$dL(t) = \sqrt{f''(1)L(t)}dW(t) + f''(1)dt \quad (4.11)$$

where we have used the fact that $\mathbb{E}[Z_0] = f''(1)$. \square

Re-scaling $L(t) \rightarrow 2L(t)/f''(1)$ gives us exactly the result found in [40].

4.2 Scaling dimensions of Ising CFT fields

Equipped with the existence of the Lamperti-Ney Process, we can now explicitly construct a Dehn twist in a random continuum CT as follows. Identify the ends of the spatial slices to obtain a space with the topology of a cylinder, where the circumference at height t is $L(t)$. Choose a curve c at height $t_0 + 1/2$ and let A be a neighbourhood of c which is homeomorphic to $S^1 \times [t_0, t_0 + 1]$. Noting that $L(t)$ is a continuous function, we define coordinates (s, t) on A where $s = e^{2\pi ix/L(t)}$, with $x \in [0, L(t)]$ and $t \in [t_0, t_0 + 1]$. Then the Dehn twist f is defined as

$$f : (e^{2\pi ix/L(t)}, t) \mapsto (e^{2\pi i(x+(t-t_0)L(t))/L(t)}, t)$$

or, in terms of the x coordinate, $x \mapsto x + (t - t_0)L(t)$. We observe that this construction does not exist for the Liouville case as the stochastic process described in section 2.5 is not continuous.

Theorem 4.3 (Scaling dimensions of Ising CFT operators). *Assume that a continuum limit of the Ising model on a CT exists, then there exist fields in the continuum CFT with spin $(L_0 - \bar{L}_0)$ given by*

- $h_\psi = 1/2 + n, n \in \mathbb{Z}$
- $h_\sigma = 1/16 + n, n \in \mathbb{Z}$

Proof. Firstly, the results of Corollary 3.2 are topological and so given the existence of a continuum limit, they persist at all scales. In the continuum, the known form of the Dehn twist operator is given by $e^{2\pi i(L_0 - \bar{L}_0)}$ and we have shown explicitly that it exists. Hence we can read off the spin of the field associated with ψ as $h_\psi = 1/2 + n, n \in \mathbb{Z}$, where we have chosen the $\lambda = -1$ sector. We are free to choose the sector because local manipulations of plaquettes prove that that the Dehn twist operators \mathbf{T}_ψ and \mathbf{T}_σ always commute with the transfer matrix. Therefore, we can label a state by the eigenvalues $\lambda_\psi, \lambda_\sigma$ and the spin configuration. Similarly for the duality defect, comparing the results of Corollary 3.2 to the continuum Dehn twist operator, we find that there is a sector where $h_\sigma = 1/16 + n, n \in \mathbb{Z}$. \square

4.3 Properties of the Lamperti-Ney process

As we showed above, the LNP is defined by

$$dL(t) = \sqrt{f''(1)L(t)} dW(t) + f''(1) dt \quad (4.12)$$

where $W(t)$ is a standard Wiener Process (WP) which has the property that

$$W_1(t) = x^{-\frac{1}{2}}W(xt) \quad (4.13)$$

$$W_2(t) = W(t+x) - W(x) \quad (4.14)$$

$$W_3(t) = tW(-t^{-1}) \quad (4.15)$$

are all WPs. In general if $g \in SL(2, R)/\{\pm 1\}$ (with the usual representation and $ad - bc = 1$) then

$$W_g(t) = (ct + d)W\left(\frac{at + b}{ct + d}\right) - ctW\left(\frac{a}{c}\right) - dW\left(\frac{b}{d}\right) \quad (4.16)$$

is also a WP.

Lemma 4.4. *If $L(t)$ is an LNP, then so is $L_x(t) = x^{-1}L(xt)$.*

Proof. From (4.12) we have

$$\begin{aligned} dL_x(t) &= d(x^{-1}L(xt)) = x^{-1}dL(xt) \\ &= \sqrt{f''(1)x^{-1}L(xt)}x^{-\frac{1}{2}}dW(xt) + f''(1)dt \\ &= \sqrt{f''(1)L_x(t)}dW_1(t) + f''(1)dt, \end{aligned} \quad (4.17)$$

where we have used (4.13). □

Now consider the ‘square’ segment of an LNP shown in figure 7, then

Lemma 4.5. *The square area $S_x(L_0) = x^{-2}S(xL_0)$, where $x > 0$, is equal in law to $S(L_0) = \int_{s=0, L(0)=L_0}^{L_0} L(s) ds$.*

Proof. Consider the scaled area process

$$S_x(L_0) = x^{-2}S(xL_0) = x^{-2} \int_{s=0, L(0)=xL_0}^{xL_0} L(s) ds. \quad (4.18)$$

Let $s = xt$, then

$$S_x(L_0) = \int_{s=0, x^{-1}L(0)=L_0}^{L_0} x^{-1}L(xt) dt. \quad (4.19)$$

Applying Lemma 4.4 to the r.h.s. then gives

$$S_x(L_0) = \int_{s=0, L_x(0)=L_0}^{L_0} L_x(t) dt, \quad (4.20)$$

which is equal in law to $S(L_0)$. □

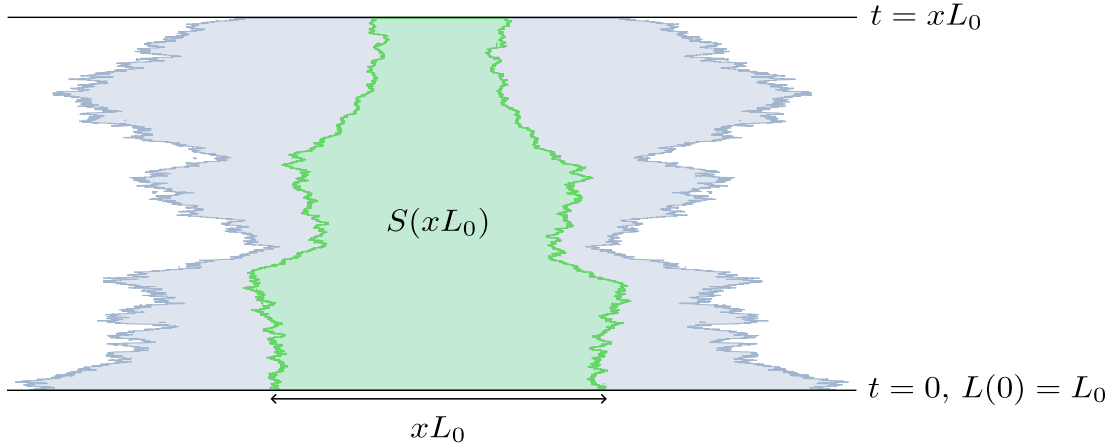


Figure 7. A segment of an LNP. The region shaded green is generated from a subset of the process at $t = 0$ and has area $S(xL_0)$.

In other words, $S(xL_0)$ is equal in law to $x^2S(L_0)$ and so scales like a canonical 2D area.

Lemma 4.6. *The process $L(t)$, $L(0) = L_0 > 0$ is strictly positive at all positive times.*

Proof. Let $L(t) = f''(1)L'(t)/4$, then

$$dL'(t) = 4dt + 2\sqrt{L'(t)}dW(t).$$

This is an $n = 4$ squared Bessel process which is strictly positive for all positive t [43]. \square

4.4 Classical and quantum scaling exponents in CDT

In this section we give another proof, in the spirit of the Duplantier-Sheffield construction, that scaling exponents on causal random geometry do not shift according to a KPZ-like relation. In the same way that DS used the volume term in the Liouville action to define a random measure $d\mu = e^{\gamma\phi}d^2z$ we can define a random measure for continuum CDTs as $d\mu = L(t)dtdx$, where $L(t)$ is a Lamperti-Ney Process (4.11). The spatial direction is uniform so we may write the two-dimensional measure as $d\mu = L(t)dt$, since the base space is $[0, 1] \times [0, 1]$. It is clear that (4.11) is Lipschitz continuous on the domain $(0, \infty)$ and so has a continuous strong solution. The solution $L(t)$ is a proper function of t so no regularization of distributions is required in contrast to the case with the Liouville measure.

We are now in a position to show that the KPZ formula does not apply to CDTs in the continuum and in fact there is no shift in the scaling dimensions of fields on CDTs compared to a fixed lattice (up to logarithmic corrections). It will be convenient to rewrite the definitions of the scaling exponents (2.22–2.23) in a discrete form. First, consider dividing the base space $[0, 1] \times [0, 1]$ in two ways:

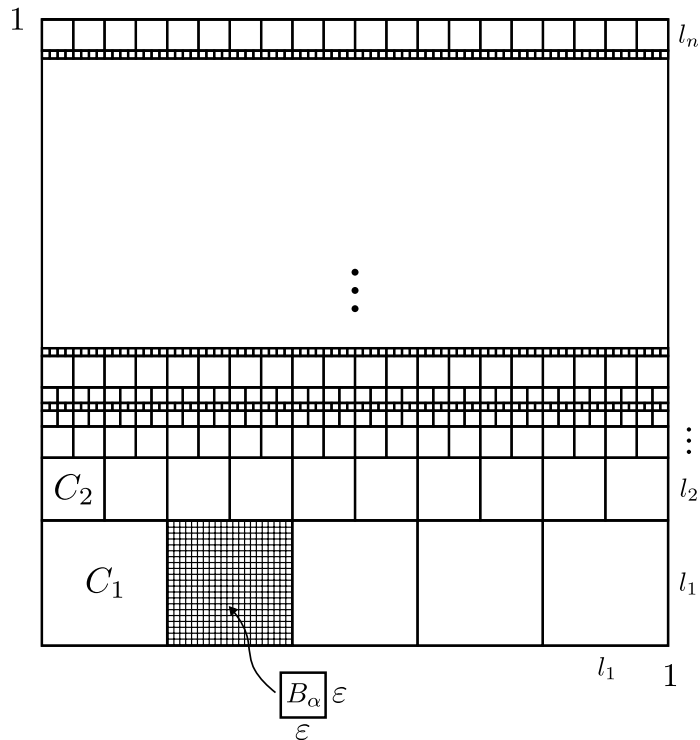


Figure 8. A dyadic decomposition of the base space $[0, 1] \times [0, 1]$ according to the measure μ .

1. Into base cells $\mathcal{B} = \{B_\alpha, \alpha = 1, \dots, 1/\varepsilon^2\}$ of classical area ε^2 , $\varepsilon \ll 1$.
2. Into quantum cells $\{C_\alpha, \alpha = 1, \dots, S(1)/\delta\}$ of quantum area δ following the dyadic decomposition procedure outlined in section 2.5, such that $\mu(C_\alpha) = \delta$. Let \mathcal{B}_α denote the set of base cells in C_α and $K_\alpha = |\mathcal{B}_\alpha|$.

Note that the dyadic decomposition according to the measure μ is much simpler than that of Liouville gravity. Due to the one-dimensional nature, the base space is divided into rows $i = 1, \dots, n$, where each quantum cell in a row is the same size in the base space and has the same quantum area – see figure 8. We use Greek subscripts when referring to an element of the complete set of cells and Latin subscripts to label the height of a cell. For example, C_i is a quantum cell at a height i in the base space – there is no need to distinguish the cell in the row, since they are all copies of each other.

Let X denote a random subset of $[0, 1] \times [0, 1]$ and $\mathcal{X} = \{b \in \mathcal{B} : b \cap X \neq \emptyset\}$ denote the set of base cells that intersect X .

Definition 4.1 (Discrete Euclidean and quantum scaling exponents).

- The **Euclidean scaling exponent** $x = x(X)$ is defined as

$$x(X) := \lim_{\varepsilon \rightarrow 0} \frac{\log \mathbb{E}_X[\varepsilon^2 N(\varepsilon, X)]}{\log \varepsilon^2} \quad (4.21)$$

where $N(\varepsilon, X)$ is the number of base cells that intersect X .

- The **quantum scaling exponent** $\Delta = \Delta(X)$ is defined as

$$\Delta(X) := \lim_{\delta \rightarrow 0} \frac{\log \mathbb{E}_X[\delta N_Q(\delta, X)]}{\log \delta} \quad (4.22)$$

where $N_Q(\delta, X)$ is the number of quantum cells that intersect X .

The expectation in both cases is over the ensemble of random subsets X .

Theorem 4.7. The quantum scaling dimension $\Delta(X)$ and the classical scaling dimension $x(X)$ are equal for the measure $d\mu = L(t)dt$, where $L(t)$ is a LNP.

Proof. Lemma 4.5 tells us that for a quantum cell, C_i at height i , $\delta = l_i^2 S_i$, where l_i is the edge length of the dyadic square in the base space and S_i is sampled from the law of $S(1)$. Hence, C_i contains $K_i = l_i^2/\varepsilon^2 = \delta/\varepsilon^2 S_i$ base grid cells. By Lemma 4.6, it follows that S_i is strictly positive $\forall i = 1, \dots, n$ and hence K_i is finite. In order to neglect any edge effects between quantum cells, we take $\delta = K\varepsilon^2$, where $K \gg 1$, so that $K_i \gg 1$, $\forall i$.

Let $p_X(\varepsilon) = \mathbb{P}[B_\alpha \cap X \neq \emptyset]$ be the *a priori* probability that X intersects a given base cell B_α , then the probability that a given quantum cell C_i at height i intersects the subset X , $\mathbb{P}[C_i \cap X \neq \emptyset]$ is given by

$$\begin{aligned} \mathbb{P}[C_i \cap X \neq \emptyset] &= \mathbb{P}[\mathcal{B}_i \cap \mathcal{X} \neq \emptyset], \\ &= 1 - \mathbb{P}[\mathcal{B}_i \cap \mathcal{X} = \emptyset], \\ &= 1 - (1 - p_X(\varepsilon))^{K_i}. \end{aligned}$$

The number of quantum cells that intersect X , $N_Q(\delta, X)$ is given by

$$N_Q(\delta, X) = \sum_{i=1}^n \frac{1}{l_i} \mathbb{P}[C_i \cap X \neq \emptyset]. \quad (4.23)$$

The quantum scaling dimension is therefore

$$\Delta(X) = \lim_{\delta \rightarrow 0} \frac{\log \mathbb{E}_X[\delta \sum_{i=1}^n \frac{1}{l_i} (1 - (1 - p_X(\varepsilon))^{K_i})]}{\log \delta}. \quad (4.24)$$

In the limit $\delta \rightarrow 0$ (equivalently $\varepsilon \rightarrow 0$), $p_X(\varepsilon)K_i$ becomes small. Hence,

$$\Delta(X) = \lim_{\delta \rightarrow 0} \frac{\log[\delta \sum_{i=1}^n \frac{K_i}{l_i} \mathbb{E}_X[p_X(\varepsilon)]]}{\log \delta}. \quad (4.25)$$

The sum $\sum_{i=1}^n \frac{K_i}{l_i} = 1/\varepsilon^2$ is the total number of base grid cells. Using $\delta = K\varepsilon^2$ and $\mathbb{E}_X[p(\varepsilon)] = \varepsilon^{2x}$, we have

$$\Delta(X) = \lim_{\varepsilon \rightarrow 0} \frac{\log K\varepsilon^{2x}}{\log K\varepsilon^2} = x(X). \quad (4.26)$$

□

We remark that this result is an inevitable outcome of the continuous, one dimensional nature of the measure.

5 Connection to Hořava-Lifshitz gravity

We note another interesting connection to projectable Hořava-Lifshitz (HL) gravity. The action for projectable HL gravity can be reduced to a one-dimensional action of the form [14]

$$S_E = \int dt \left(\frac{\dot{L}(t)^2}{4L(t)} + \Lambda L(t) \right). \quad (5.1)$$

We will show that this is related to the Lamperti-Ney Process.

The Onsager-Machlup (OA) function allows us to write down a Lagrangian associated to any SDE [44–46]. In general, for an Itô process

$$dX_t = f(X_t)dt + \sigma(X_t)dW_t \quad (5.2)$$

the OA function is given by

$$\mathcal{L}(\dot{x}, x) = \frac{(\dot{x} - f(x))^2}{2\sigma(x)^2}. \quad (5.3)$$

In our case, for the Lamperti-Ney Process, the OA function is given by

$$\mathcal{L}(\dot{L}, L) = \frac{(\dot{L} - 2)^2}{4L}, \quad (5.4)$$

where we have scaled $L(t) \rightarrow L(t)/f''(1)$. The associated formal path integral to the OA Lagrangian is

$$Z = \int \mathcal{D}L e^{-\int \mathcal{L}(\dot{L}, L) dt}. \quad (5.5)$$

As is standard procedure in the probabilistic approach to quantum field theory (see [36]), we interpret the term

$$Z^{-1} e^{-\int \mathcal{L}(\dot{L}, L) dt} \mathcal{D}L \quad (5.6)$$

as the measure which properly weighs the paths given by the stochastic process.

We are often interested in adding potential terms to the Lagrangian, such as a cosmological constant term. These are then considered as observables whose expectation is being calculated with respect to the measure (5.6). For example, adding a cosmological constant term would look like

$$\int \mathcal{D}L e^{-\int \mathcal{L}(\dot{L}, L) + \Lambda L dt} = \mathbb{E}[e^{-\Lambda \int dt L}] \quad (5.7)$$

where \mathbb{E} is over paths sampled according to the SDE. This is indeed the correct cosmological constant term since $\int dt L(t)$ is the two dimensional volume. For a general observable $F(L)$ this would be

$$\int \mathcal{D}L F(L) e^{-\int \mathcal{L}(\dot{L}, L) dt} = \mathbb{E}[F(L)]. \quad (5.8)$$

Equation (5.8) may remind the reader of the expression that satisfies the Feynman-Kac formula. Indeed, if we specify an initial condition, say $L_0 = l$, then $\phi(l, \tau) = \mathbb{E}[G(L) e^{-\Lambda \int^\tau dt L} | L_0 = l]$ satisfies the differential equation

$$-\frac{\partial \phi}{\partial \tau} = -L \frac{\partial^2 \phi}{\partial L^2} - 2 \frac{\partial \phi}{\partial L} + \Lambda L; \quad \phi(l, 0) = G(l), \quad (5.9)$$

which is exactly the imaginary time Schrödinger equation with the CDT Hamiltonian [7, 40].

The form of the Lagrangian is almost exactly (5.4) but without the “ -2 term”. We can reconcile this difference by considering the associated Hamiltonian to the HL action. As discussed in [14] the HL Hamiltonian is given by $H = L\Pi^2 + \Lambda L$. However, there is an operator ordering ambiguity that is resolved by choosing different measures such that H is Hermitian. These different choices of measure also have a combinatorial origin corresponding to the marking/unmarking of entry boundaries [14]. Choosing the measure LdL gives us the Hamiltonian $H = -\frac{\partial^2}{\partial L^2} L + \Lambda L$ which is exactly (5.9). This further corroborates the findings that 2D continuum CDT is 2D Projectable Hořava-Lifshitz gravity, this time showing the correspondence from the other direction.

6 Outlook and extension to the annealed case

In the quenched model, where a graph is first sampled from the UICCT ensemble, and matter fields are subsequently placed on it, we have demonstrated that there is no change in the critical exponents compared to the flat lattice for any height model. In the particular case of the Ising model, Theorem 4.3 corroborates the numerical results in [9, 47, 48]. If a critical point exists, the topological defects and their associated fusion algebra persist in the continuum, being independent of

any coupling constant. The continuity of the stochastic process $L(t)$, guarantees the existence of the Dehn twist in the continuum. Hence, the discrete arguments apply, showing that the conformal dimensions of the Ising operators are unchanged from their Onsager values.

This is in contrast to the KPZ relation in Liouville gravity, where even in the pure gravity case ($\gamma = \sqrt{8/3}$) we get a non-trivial relation between $x(X)$ and $\Delta(X)$. One way to explain this difference between causal and Euclidean random geometry is that there is no clear way to define a Dehn twist in the Euclidean setting. In the discrete Euclidean picture, the set of vertices at a constant geodesic distance from a chosen origin is almost surely disconnected. The Dehn twist cannot be defined because there is no curve around which there exists a region homeomorphic to $S^1 \times [0, 1]$, due to the fractal nature of the space. All that is to say, the unique properties of causal random geometry allow us to readily extend the arguments in [12, 37] to CTs but not to Euclidean triangulations.

In the *annealed model*, which amounts to sampling a graph $C \in \mathcal{C}_\infty$ according to the measure $\mu_J(C)$, we do not know the exact form of the process that describes the evolution of the random geometry. However, we do know that it must be described by some one-dimensional stochastic process $X(t)$, due to the restriction to causal graphs with a global time foliation. It follows that, to extend our arguments to the annealed model, it would be sufficient to prove the continuity of $X(t)$. This argument applies to any coupling of unitary matter to CDT if a second order phase transition exists, where a continuum limit can be defined.

Another interesting observation comes from the functional renormalization group equation (FRGE) analysis of the matrix model representation of CDT [49]. The authors find that the anomalous dimension vanishes due to the presence of the matrices C (not to be confused with the causal graph) that impose the causal structure in the ribbon graphs. Since it is exactly the anomalous dimension that shifts the scaling exponents, it follows that there should be no KPZ-like relation. The same analysis of the Ising-CDT matrix model defined in [50] comes to the same conclusion [51]. In fact, it is clear that any matrix model description of CDT coupled to matter that uses these C matrices to impose the causal constraint will contain vanishing anomalous dimensions.

Acknowledgments

We thank Davide Laurenzano for insightful comments on the matrix model representation. We would also like to thank Isaac Layton for useful discussions and for introducing the Onsager-Machlup function. Ryan Barouki is supported by STFC studentship ST/W507726/1 and Henry Stubbs is supported by STFC studentship ST/X508664/1. For the purpose of open access, the authors have applied a CC BY

A Defects at the boundary

One is free to choose boundary conditions as part of the definition of the partition function. Two choices are *free* and *fixed*. In the free case, the boundary spins are summed over in the partition function just like any other bulk spin. In the fixed case, the boundary is defined by a state $|B\rangle = |\dots 0001101011\dots\rangle$ for example, which specifies the spin at every boundary vertex. We are interested in whether a defect is free to move at the boundary without altering the partition function. Figure 9 shows the boundary spins a, b, c, d in the presence of a spin defect. Notice that the final plaquettes are horizontal to signify that an edge joins the boundary points.

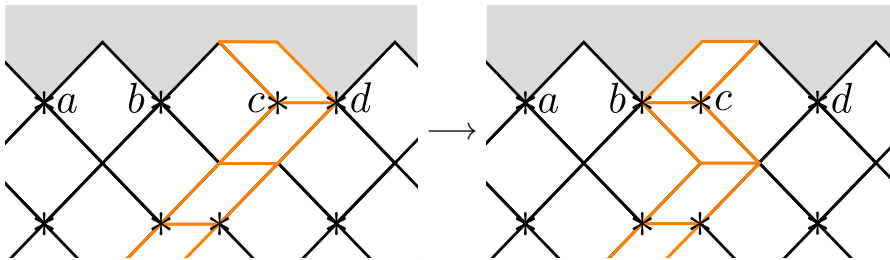


Figure 9. Spin defect ending at the boundary (top) being moved one spin to the left. The boundary spins are those marked a, b, c, d .

If the boundary conditions are free, then by the same bulk moves in (3.6–3.7), a spin defect move at the boundary is also topological. On the other hand, suppose we fix the boundary such that $a = 0, b = 0, c = 1, d = 1$, then before the move, the section of the boundary shown in figure 9 contributes a factor $W^H(u)_{00}W^H(u)_{11} \times 1$, where the factor of 1 comes from the spin defect. After the move the contribution is $W^H(u)_{00}W^H(u)_{10} \times 0$, where the factor of 0 also comes from the spin defect but with the same spin on each side of the plaquette. Hence it is clear that this move does not preserve the partition function and is not topological.

The case of the duality defect is slightly trickier – consider the diagram in figure 10. The left-hand side of the figure contributes a factor

$$W^H(u_H)_{ab}(-1)^{bd}(-1)^{bc}, \quad (\text{A.1})$$

whereas the right-hand side is given by

$$W^V(u_H)_{bd}(-1)^{ad}(-1)^{ab}. \quad (\text{A.2})$$

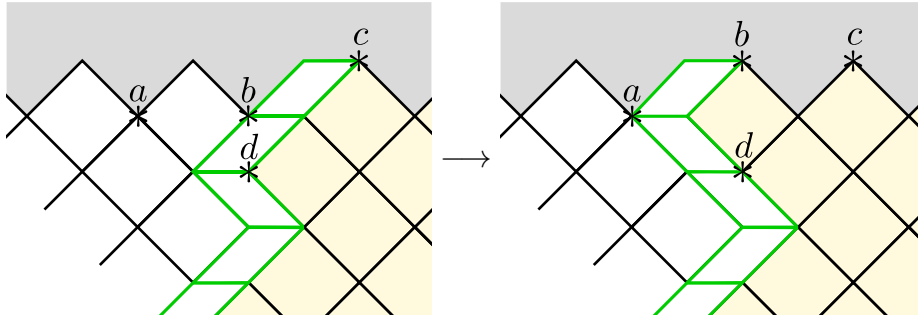


Figure 10. Moving a duality defect at the boundary (top) one step to the left. The boundary spins are a, b, c . The yellow shading shows the difference between the dual and original plaquettes.

Let's first consider free boundary conditions. This amounts to summing over b since this is the only internal spin in the diagram. By evaluating \sum_b (A.1) and \sum_b (A.2), one finds that the duality defect cannot be moved without changing the partition function for all values of u_H, u_V . Now consider a magnetised boundary with $a = b = c = 0$. In this case, by evaluating the diagram on both sides, we again find that the duality defect cannot be moved freely for all values of u_H and u_V . Therefore, we have shown that it is possible to pin any defect to the boundary by choosing suitable boundary conditions.

B The domain wall

As we alluded to in Section 3, when considering a vertical duality defect in a space with periodic boundary conditions, we necessarily require a domain wall where the dual lattice meets the original again. In this appendix, we will elaborate on the details of the wall and show that defects can pass through the wall topologically.

One way to implement the wall is to introduce a new plaquette that identifies the spins at the wall. This plaquette is defined as

$$\begin{array}{c} \bullet \\ \hline \ast a \\ \hline \bullet \\ \hline \ast b \end{array} = \delta_{ab}, \tag{B.1}$$

and Figure 11 shows how it is implemented at the interface of the original and dual lattices.

Consider a horizontal sequence of duality defect plaquettes, such as those that constitute the Dehn twist in the presence of a vertical duality defect. At some point, there will be an intersection of the horizontal plaquettes with the wall, as shown in Figure 12. Notice that at the intersection of the wall and the horizontal defect, there

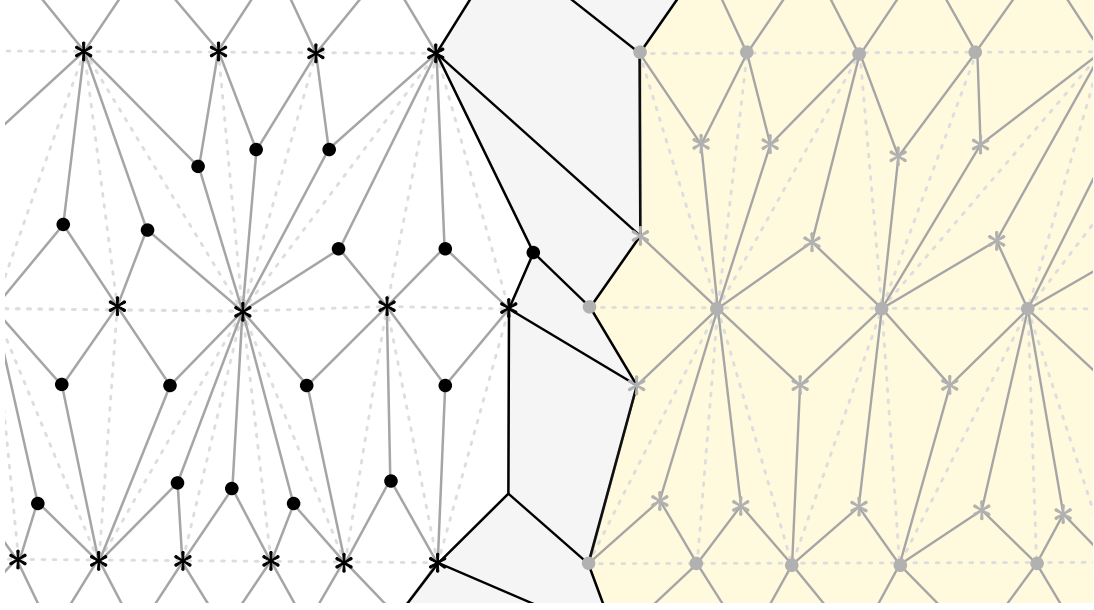


Figure 11. The domain wall where the original and dual lattice meet again in the presence of a vertical duality defect. Black asterisks indicate the positions of the spins on G , while gray asterisks mark the positions of the spins on G^* . Black dots denote empty positions in G , and gray dots denote empty positions in G^* . The dotted lines depict the underlying triangulation.

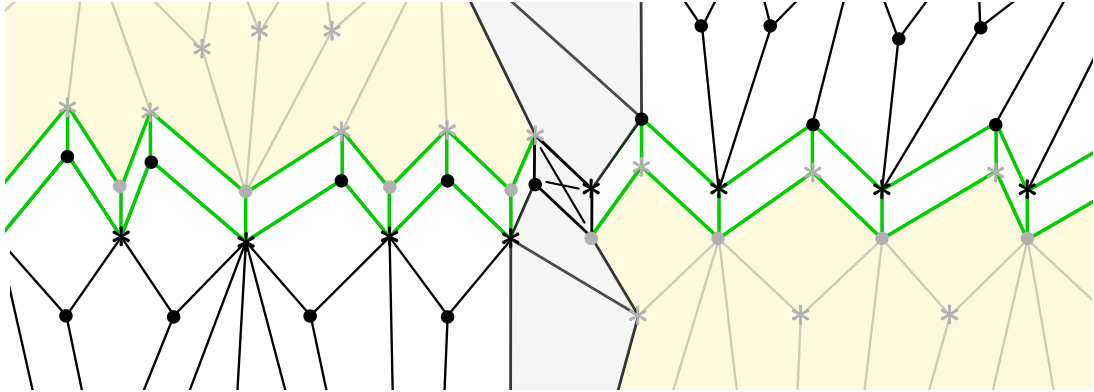


Figure 12. The intersection of a horizontal duality defect and the domain wall.

is a new type of object

$$\begin{array}{c}
 \bullet \\
 \hline
 \bullet
 \end{array}
 \begin{array}{c}
 \ast a \\
 \hline
 \ast b
 \end{array}
 = \delta_{ab}
 \tag{B.2}$$

which is almost identical to (B.1) but differs with the relative positions of the original and dual empty sites.

The question is whether the horizontal defect can be moved along the wall and

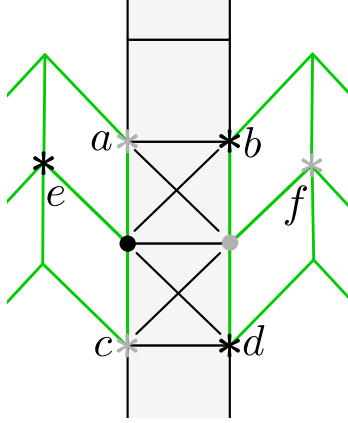


Figure 13. Two horizontal duality defects meeting at the wall.

what happens when two horizontal defects meet at the wall. To answer the first question, consider the following diagram

Evaluating the left-hand side,

$$\begin{aligned}
 &= 2^{-1/2}(-1)^{ac} \times 2^{-1/2}(-1)^{bd} \times \delta_{ab}\delta_{cd} \times 2^{1/2} \times 2^{1/2} \\
 &= (-1)^{ac}(-1)^{bd}\delta_{ab}\delta_{cd} = \delta_{ab}\delta_{cd}
 \end{aligned}
 \tag{B.4}$$

where the final factors of $\sqrt{2}$ come from the additional blank vertices on the left-hand side compared to the right-hand side. The right-hand side of (B.3) gives the same result. Therefore, we have shown that the duality defect can be moved along the wall without obstruction. Finally, we must show what happens when two horizontal duality defects meet at the wall. Consider the diagram in Figure 13, as was shown in [12] when two duality defects meet, it is equivalent to the sum of an identity and a spin defect.

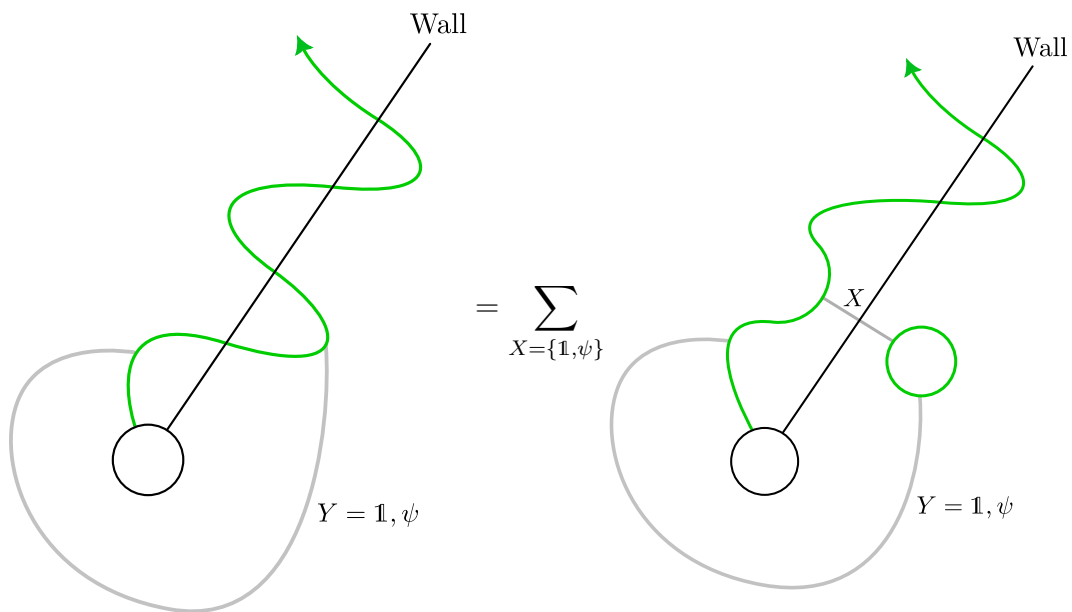


Figure 14. Macroscopic view of applying (B.5) to the set up in Section 3.5. If $Y = \mathbb{1}$, the non-zero contribution is the identity defect passing through the wall. Otherwise, if $Y = \psi$, then the spin defect passes through the wall.

$$\begin{aligned}
 \begin{array}{c} \bullet \\ \hline \sigma \\ \hline c * \\ \hline \sigma \\ \hline \bullet \end{array} &= \frac{1}{\sqrt{2}} \left[\begin{array}{c} \bullet \\ \hline \psi \\ \hline c * \\ \hline \bullet \end{array} + \begin{array}{c} \bullet \\ \hline \mathbb{1} \\ \hline c * \\ \hline \bullet \end{array} \right] \\
 &= \frac{1}{\sqrt{2}} [\delta_{ab} + \sigma_{ab}^x]
 \end{aligned} \tag{B.5}$$

Since the spins across the wall are identified, the only non-zero contributions are those in which there is either an identity or a spin defect on both sides of Figure 13. Contributions where there is an identity on one side but a spin on the other vanish.

We are interested in whether we can perform the topological moves needed at the end of Section 3 in the presence of a wall. In this setup, a single duality defect crosses the wall multiple times, as shown in Figure 14. As we concluded above, merging two duality lines at the wall produces a sum over an identity defect and a spin defect that passes through the wall. Depending on the type of defect that wraps around the centre of the space, either the identity or the spin defect will pass through the wall as shown in Figure 14. In each case, the remaining duality bubble shrinks to zero, contributing a factor of $\sqrt{2}$ which cancels the factor in the sum in (B.5). Hence, we have shown that the duality defect can be moved through the wall, allowing us to perform the necessary moves in calculating the conformal dimensions in Section 3.5.

References

- [1] B. Duplantier, *Random walks and quantum gravity in two dimensions*, *Phys. Rev. Lett.* **81** (1998) 5489.
- [2] V.G. Knizhnik, A.M. Polyakov and A.B. Zamolodchikov, *Fractal Structure of 2D Quantum Gravity*, *Mod. Phys. Lett. A* **3** (1988) 819.
- [3] F. David, *Conformal Field Theories Coupled to 2D Gravity in the Conformal Gauge*, *Mod. Phys. Lett. A* **3** (1988) 1651.
- [4] J. Distler and H. Kawai, *Conformal field theory and 2d quantum gravity*, *Nuclear Physics B* **321** (1989) 509.
- [5] V. Kazakov, *Ising model on a dynamical planar random lattice: Exact solution*, *Physics Letters A* **119** (1986) 140.
- [6] D.V. Boulatov and V.A. Kazakov, *The Ising Model on Random Planar Lattice: The Structure of Phase Transition and the Exact Critical Exponents*, *Phys. Lett. B* **186** (1987) 379.
- [7] J. Ambjørn and R. Loll, *Non-perturbative lorentzian quantum gravity, causality and topology change*, *Nuclear Physics B* **536** (1998) 407–434.
- [8] J. Ambjørn, K.N. Anagnostopoulos and R. Loll, *New perspective on matter coupling in 2d quantum gravity*, *Physical Review D* **60** (1999) .
- [9] J. Ambjørn, K. Anagnostopoulos, R. Loll and I. Pushkina, *Shaken, but not stirred—potts model coupled to quantum gravity*, *Nuclear Physics B* **807** (2009) 251.
- [10] J. Ambjørn, K. Anagnostopoulos and R. Loll, *Crossing the $c=1$ barrier in 2d lorentzian quantum gravity*, *Physical Review D* **61** (2000) 44010.
- [11] J.F. Wheeler and P.D. Xavier, *The cylinder amplitude in the hard dimer model on 2d causal dynamical triangulations*, *Classical and Quantum Gravity* **39** (2022) 075004.
- [12] D. Aasen, R.S.K. Mong and P. Fendley, *Topological defects on the lattice: I. the ising model*, *Journal of Physics A: Mathematical and Theoretical* **49** (2016) 354001.
- [13] B. Duplantier and S. Sheffield, *Liouville quantum gravity and kpz*, *Inventiones mathematicae* **185** (2011) 333.
- [14] J. Ambjørn, L. Glaser, Y. Sato and Y. Watabiki, *2d cdt is 2d hořava–lifshitz quantum gravity*, *Physics Letters B* **722** (2013) 172–175.
- [15] T.E. Regge, *General relativity without coordinates*, *Il Nuovo Cimento (1955-1965)* **19** (1961) 558.
- [16] W.T. Tutte, *A census of hamiltonian polygons*, *Canadian Journal of Mathematics* **14** (1962) 402 .
- [17] W.T. Tutte, *A census of planar triangulations*, *Canadian Journal of Mathematics* **14** (1962) 21 .

- [18] W.T. Tutte, *A census of slicings*, *Canadian Journal of Mathematics* **14** (1962) 708 .
- [19] W.T. Tutte, *A census of planar maps*, *Canadian Journal of Mathematics* **15** (1963) 249 .
- [20] V. Kazakov, I. Kostov and A. Migdal, *Critical properties of randomly triangulated planar random surfaces*, *Physics Letters B* **157** (1985) 295.
- [21] F. David, *A model of random surfaces with non-trivial critical behaviour*, *Nuclear Physics B* **257** (1985) 543.
- [22] E. Brezin, C. Itzykson, G. Parisi and J.B. Zuber, *Planar Diagrams*, *Commun. Math. Phys.* **59** (1978) 35.
- [23] D. Anninos and B. Mühlmann, *Notes on matrix models (matrix musings)*, *J. Stat. Mech.* **2008** (2020) 083109 [2004.01171].
- [24] J.-F. Gall, *The topological structure of scaling limits of large planar maps*, *Inventiones mathematicae* **169** (2006) .
- [25] J.-F.L. Gall, *Uniqueness and universality of the Brownian map*, *The Annals of Probability* **41** (2013) 2880 .
- [26] J. Bettinelli, “Planar map with 30,000 vertices.”
- [27] R. Sorkin, *Time-evolution problem in regge calculus*, *Phys. Rev. D* **12** (1975) 385.
- [28] J. Ambjørn, L. Glaser, Y. Sato and Y. Watabiki, *2d CDT is 2d Hořava–Lifshitz quantum gravity*, *Phys. Lett. B* **722** (2013) 172 [1302.6359].
- [29] M. Krikun and A. Yambartsev, *Phase transition for the ising model on the critical lorentzian triangulation*, *J Stat Phys* **148** (2008) 422–439 [0810.2182].
- [30] B. Durhuus, T. Jonsson and J. Wheeler, *From trees to gravity*, in *Handbook of Quantum Gravity*, C. Bambi, L. Modesto and I. Shapiro, eds., (Singapore), pp. 3385–3435, Springer Nature Singapore (2024), DOI.
- [31] B. Durhuus, T. Jonsson and J.F. Wheeler, *On the spectral dimension of causal triangulations*, *J. Statist. Phys.* **139** (2010) 859 [0908.3643].
- [32] B. Durhuus, *Probabilistic Aspects of Infinite Trees and Surfaces*, *Acta Physica Polonica B* **34** (2003) 4795.
- [33] A. Polyakov, *Quantum geometry of bosonic strings*, *Physics Letters B* **103** (1981) 207.
- [34] J. Teschner, *Liouville theory revisited*, *Classical and Quantum Gravity* **18** (2001) R153–R222.
- [35] Y. Nakayama, *Liouville field theory: A Decade after the revolution*, *Int. J. Mod. Phys. A* **19** (2004) 2771 [hep-th/0402009].
- [36] F. Guerra, L. Rosen and B. Simon, *The $p(\phi)_2$ euclidean quantum field theory as classical statistical mechanics*, *Annals of Mathematics* **101** (1975) 111.

- [37] D. Aasen, P. Fendley and R.S.K. Mong, *Topological defects on the lattice: Dualities and degeneracies*, [2008.08598](#).
- [38] J.L. Cardy, *Boundary conditions, fusion rules and the verlinde formula*, *Nuclear Physics B* **324** (1989) 581.
- [39] J. Lamperti and P. Ney, *Conditioned branching processes and their limiting diffusions*, *Theory of Probability & Its Applications* **13** (1968) 128 [<https://doi.org/10.1137/1113009>].
- [40] V.V. Sisko, A. Yambartsev and S. Zohren, *A note on weak convergence results for infinite causal triangulations*, *Brazilian Journal of Probability and Statistics* (2018) .
- [41] S.N. Ethier and T.G. Kurtz, *Markov processes – characterization and convergence*, Wiley Series in Probability and Mathematical Statistics: Probability and Mathematical Statistics, John Wiley & Sons Inc., New York (1986).
- [42] T.G. Kurtz and P. Protter, *Weak Limit Theorems for Stochastic Integrals and Stochastic Differential Equations*, *The Annals of Probability* **19** (1991) 1035 .
- [43] D. Revuz and M. Yor, *Continuous Martingales and Brownian Motion*, Grundlehren der mathematischen Wissenschaften, A Series of Comprehensive Studies in Mathematics, 293, Springer Berlin Heidelberg, Berlin, Heidelberg, 3rd ed. 1999. ed. (1999).
- [44] L. Onsager and S. Machlup, *Fluctuations and irreversible processes*, *Phys. Rev.* **91** (1953) 1505.
- [45] W. Horsthemke and A. Bach, *Onsager-Machlup Function for one dimensional nonlinear diffusion processes*, *Zeitschrift für Physik B Condensed Matter* **22** (1975) 189.
- [46] M.F. Weber and E. Frey, *Master equations and the theory of stochastic path integrals*, *Reports on Progress in Physics* **80** (2017) 046601.
- [47] J. Ambjørn, K.N. Anagnostopoulos and R. Loll, *New perspective on matter coupling in 2d quantum gravity*, *Physical Review D* **60** (1999) .
- [48] D. Benedetti and R. Loll, *Unexpected spin-off from quantum gravity*, *Physica A: Statistical Mechanics and its Applications* **377** (2007) 373.
- [49] A. Castro and T. Koslowski, *Renormalization group approach to the continuum limit of matrix models of quantum gravity with preferred foliation*, *Frontiers in Physics* **9** (2021) [[2008.10090](#)].
- [50] J.L.A. Abranches, A.D. Pereira and R. Toriumi, *Dually weighted multi-matrix models as a path to causal gravity-matter systems*, *Annales Henri Poincaré* (2024) [[2310.13503](#)].
- [51] R. Barouki and D. Laurenzano, *To appear* (2025) .